Mechanisms of synergistic Mediator recruitment in RNA polymerase II transcription activation revealed by single-molecule fluorescence

Daniel H. Zhou[1,†], Jongcheol Jeon[2,†], Nida Farheen[1], Larry J. Friedman[1], Jane Kondev[3], Stephen Buratowski[2,*], and Jeff Gelles[1,*]

[†] These authors contributed equally to this work
[1] Department of Biochemistry, Brandeis University, Waltham, MA 02453
[2] Department of Biological Chemistry and Molecular Pharmacology, Harvard Medical School, Boston, MA 02115
[3] Department of Physics, Brandeis University, Waltham, MA 02453
[*] Correspondence: steveb@hms.harvard.edu (S.B.); gelles@brandeis.edu (J.G.)

Transcription activators trigger transcript production by RNA Polymerase II (RNApII) via the Mediator coactivator complex. Here the dynamics of activator, Mediator, and RNApII binding at promoter DNA were analyzed using multi-wavelength single-molecule microscopy of fluorescently labeled proteins in budding yeast nuclear extract. Binding of Mediator and RNApII to the template required activator and an upstream activator sequence (UAS), but not a core promoter. While Mediator and RNApII sometimes bind as a pre-formed complex, more commonly Mediator binds first and subsequently recruits RNApII to form a preinitiation complex precursor (pre-PIC) tethered to activators on the UAS. Interestingly, Mediator occupancy has a highly non-linear response to activator concentration, and fluorescence intensity measurements show Mediator preferentially associates with templates having at least two activators bound. Statistical mechanical modeling suggests this "synergy" is not due to cooperative binding between activators, but instead occurs when multiple DNA-bound activator molecules simultaneously interact with a single Mediator.

Keywords

TIRF; synergy; statistical mechanics; CoSMoS; activation domain; intrinsically disordered region

Introduction

Eukaryotic genes respond to a wide range of cues. Multicellular plants and animals contain dozens to hundreds of differentiated cell types, each expressing distinct subsets of the same genomic information[1,2]. Even single-cell eukaryotes such as yeast exhibit a wide range of specific transcription patterns tuned to nutrient availability, temperature, and other environmental conditions. A major determinant of these complex patterns of gene expression are transcription activators (TAs), sequence-specific DNA binding proteins that promote assembly of the RNA Polymerase II (RNApII) transcription machinery to form a pre-initiation complex (PIC) on target promoters[3–5]. More complete understanding of the molecular mechanisms of transcription activation remains an essential goal in understanding eukaryotic gene regulation.

Binding sites for TAs are typically clustered within DNA elements known as enhancers or upstream activating sequences (UASs)[6]. Metazoan enhancers often have a dozen or more TA binding sites[1]. Early promoter analyses showed that two or more binding sites for the same TA can result in far greater activation than the sum of that from the individual sites, a phenomenon termed "synergy"[7–9]. More generally, enhancers with sites for different TAs can synergistically integrate different signals transmitted through these distinct TAs, providing a basis for combinatorial regulation of promoters[4,10–12]. However, multiple TA sites in an enhancer do not always produce synergy[12–15], and multiple mechanisms for synergy have been proposed[9,14,16–19].

TAs bound at a UAS promote assembly of PICs at the core promoter through multiple coactivators. Chromatin modifying and remodeling coactivators (e.g., SAGA, SWI/SNF) modulate promoter accessibility. However, the most critical coactivator may be Mediator[20–24]. This large, multi-subunit complex has Head and Middle modules that can bind RNApII and several general transcription factors (GTFs); a Tail module that can bind the activation domains of many TAs; and a reversibly-associating kinase module that can phosphorylate TAs[24–30]. These interactions are believed to "mediate" communication between UAS-bound TAs and PIC components at the core promoter. This role is consistent with chromatin immunoprecipitation experiments detecting Mediator presence at either enhancers or at core promoters depending on the circumstances[28,31–34]. Likewise, structural studies have provided static pictures showing Mediator incorporated into either the PIC at the core promoter[35–39] or bound with TAs, RNApII, and some GTFs at the UAS[40]. Finally, in vivo imaging experiments have led to models where clusters of multiple Mediator molecules form condensates at enhancers via intrinsically disordered regions[41,42]. Given this

diversity of its interactions, structural poses, and functions, the molecular mechanisms by which Mediator conveys activating signals from TAs to the PIC machinery at core promoters are still not well understood[31,43–45].

Functional mechanisms of systems capable of multiple macromolecular interactions are often best revealed by single-molecule methods. We used colocalization single-molecule spectroscopy (CoSMoS)[46,47] to directly image TA, RNApII, and Mediator dynamics on individual DNA molecules in real time. Our experiments are based on budding yeast (*Saccharomyces cerevisiae*) nuclear extracts which contain the full complement of nuclear proteins and recapitulate the essential features of activated transcription in vitro[48–51] when supplemented with the recombinant TA Gal4-VP16[52–54]. To focus solely on chromatin-independent transcription activation mechanisms, the template DNA was not pre-assembled into chromatin.

Using this system, we previously found[49] that RNApII and GTFs do not sequentially assemble PICs directly on the core promoter as often assumed. Instead, RNApII, TFIIF, and TFIIE associate first at the TA-bound UAS to form a PIC precursor (pre-PIC), which we proposed then transfers to the core promoter. Here we define the role of Mediator in PIC formation by showing that Mediator also initially binds UAS-associated TAs independently of the core promoter, and that this binding is necessary for simultaneous or subsequent RNApII binding. Quantitative analysis of Mediator and TA occupancy on DNA reveals that a single Mediator strongly prefers templates bound by multiple TAs, and the data implicate Mediator recruitment as a locus of TA synergy.

Results

Dynamics of Gal4-VP16 and Mediator binding to DNA

We established a single-molecule fluorescence assay to characterize how UAS-bound TAs affect Mediator dynamics. TA binding was monitored using a recombinant Gal4-SNAP-VP16 protein consisting of the *Saccharomyces cerevisiae* Gal4 DNA-binding domain, a SNAP tag fluorescently labeled with red-excited dye adduct SNAP-Surface-649, and the potent herpes simplex virus VP16 transactivation domain (TAD)[51,52] (**Figure S1A**). This construct is designated below as Gal4-VP16^{649}. The DNA template contains a UAS comprised of five Gal4 binding sites positioned upstream of the *CYC1* core promoter (UAS+promoter; **Figure 1A**; **Table S4**). We confirmed that transcription from this template in yeast nuclear extract (YNE) is as strongly activated by Gal4-SNAP-VP16[51] as by Gal4-VP16[49,50,55,56] . To observe Mediator, a *S. cerevisiae* strain (YSB3613; **Table S1**) was constructed

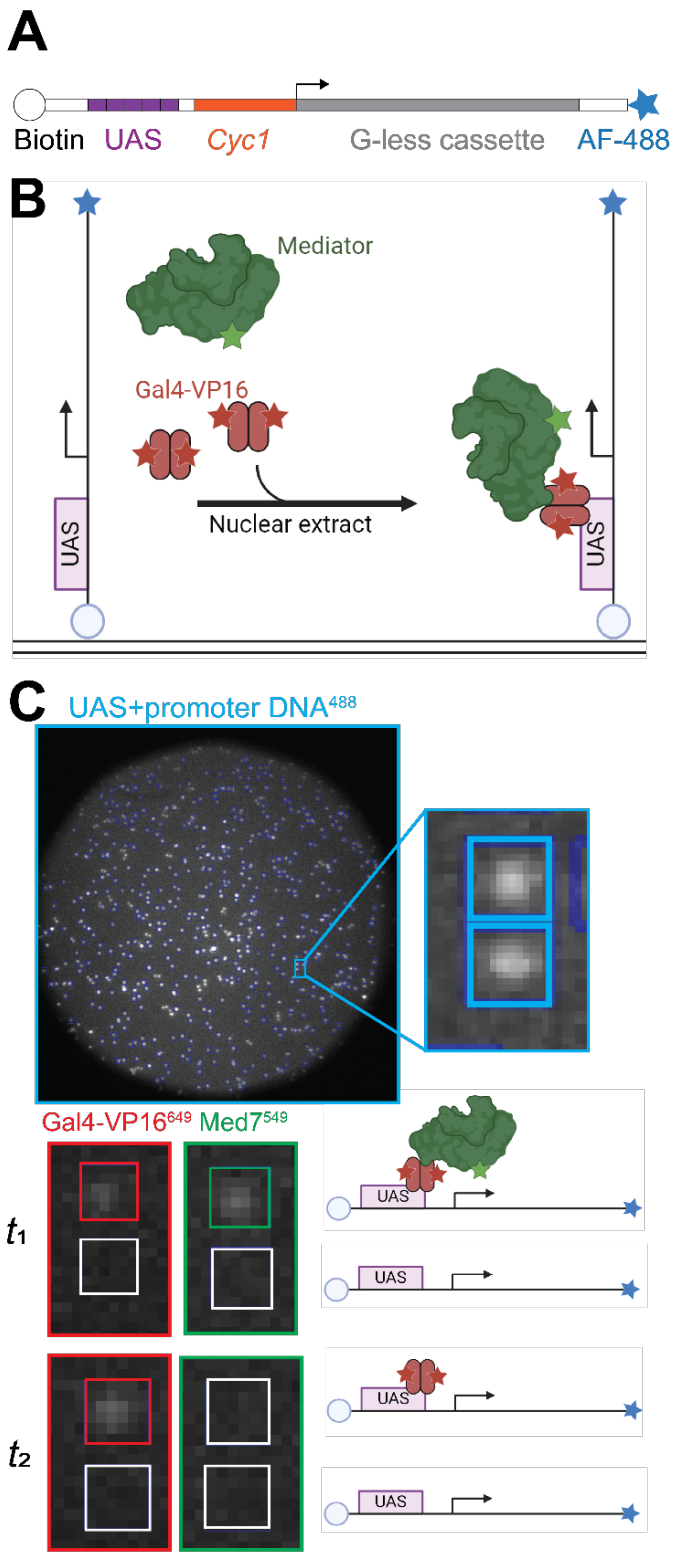

Figure 1: CoSMoS experiments design and example data. (A) Schematic of the UAS+promoter DNA. **(B)** Experimental design. Labeled Gal4-VP16^{649} (red) and Med7^{549} (green) in YNE were allowed to bind to dye-labeled UAS+promoter DNA tethered to the slide surface. **(C)** Single-molecule imaging example. Large grayscale image shows the microscope field of view (65 μm diameter) imaged for DNA before addition of extract at time t = 0. Insets show a magnified region of the field with two DNA molecules (boxes). Different laser excitation wavelengths visualized the DNA (blue border; t < 0) and colocalized Gal4-VP16^{649} (red border) or Med7^{549} (green border) at times t_1 = 101 s and t_2 = 301 s after extract addition. Cartoons illustrate inferred molecular species present on the two DNA molecules at times t_1 and t_2.

with tandem HA-tag and SNAP-tag fused to the C-terminus of Med7. Med7 is essential for viability[38], so the unperturbed growth of this strain compared to the parental strain (**Figure S1B**) suggests that the tagged Mediator functions normally *in vivo*. Western blots of the YNE from this strain confirmed expression of Med7-HA-SNAP protein at the expected molecular weight (**Figure S1C**), and the YNE treated with the green-excited dye adduct SNAP-Surface-549 shows a single fluorescent protein (hereafter abbreviated as Med7^{549}) at the same position **(Figure S1D**). Bulk transcription assays confirm that the Med7^{549}-containing YNE displays activator-dependent transcription activity *in vitro* (**Figure S1E**).

Single-molecule microscopy experiments were done using conditions previously developed[49–51] to study PIC formation (**Figure 1B**). UAS+promoter DNA templates, tagged with biotin and blue-excited dye AF488, were tethered in a neutravidin-derivatized microscope flow chamber[46,47]. Total internal reflection fluorescence (TIRF) microscopy revealed several hundred DNAs in a typical field of view (**Figure 1C**). These were incubated with Med7^{549}-containing YNE and Gal4-VP16^{649} in the absence of NTPs, conditions allowing stable formation of transcription-competent PICs while preventing transcription initiation[48–50,55].

At 10 nM Gal4-VP16^{649}, substantial binding was seen at DNA molecule locations (**Figure 2A, S2A** upper panel). These TA molecules remained bound for up to hundreds of seconds, consistent with kinetically stable binding of Gal4-VP16 to its target site. In contrast, randomly selected control locations on the slide surface that lacked labeled DNA molecules displayed little TA binding (**Figure 2B** and **Figure S2A** lower panel; only 8% (28 of 356) of control no-DNA locations showed instances of TA binding vs. 74% (376 of 506) of DNA locations). Thus, TA bound specifically to the DNA rather than non-specifically to the slide surface.

Gal4 binds its DNA target site as a dimer[57], and in some records there were two different sizes of Gal4-VP16^{649} fluorescence intensity steps (e.g., **Figure 2A**, middle trace; compare steps denoted with single and double dots), consistent with TA dimers carrying either one or two active dyes. Quantitative analysis of the step increase intensity distributions (**Figure S3A**) confirmed that 97 ± 4% (S.E.) of TA dimers were labeled with at least one dye (see Methods). At a higher Gal4-VP16^{649} concentration (50 nM, **Figure 2C**), the initial TA association to a DNA molecule was followed by additional stepwise increases in fluorescence intensity, indicating sequential binding of two or more TA molecules to the five Gal4 binding sites. At 50 nM activator, the progressive accumulation of TA molecules on individual DNAs suggests that the rate of TA binding initially outpaced the rate of departure, but eventually tended toward an equilibrium balance between arrival and departure.

In the same experiments imaging TA binding, Mediator binding was simultaneously monitored. Mediator binding was DNA-specific, with little association with control no-DNA locations (e.g., **Figure 2B; Figure S2B**: 79% (502 of 637) of DNA locations showed Mediator binding versus only 10% (56 of 561) of control locations). Surprisingly, at 10 nM Gal4-VP16^{649}, Med7^{549} binding to DNA was rare, and individual binding events were short, on the order of 1 s duration (e.g., **Figure 2A)**. In contrast, at 50 nM activator concentration, Mediator binding was more frequent and the time intervals during which Mediator was present on DNA were typically 10- to 100-fold longer (e.g., **Figure 2C**). Thus, TA concentration had a profound effect on Mediator presence on the DNA.

Even at 50 nM activator, a single DNA usually contained only one Mediator at a time, even when multiple TA molecules were simultaneously present (e.g., **Figure 2C**, red bars). Instances of multiple Mediator molecules bound simultaneously at the same DNA were rare and brief (e.g., **Figure 2C**, green bar in bottom record). There were almost no observations of multiple Mediator molecules arriving simultaneously, arguing that multimolecular Mediator condensates do not form in this experimental system, in contrast to what is reported for some mammalian enhancers in vivo[3,41,42].

TA presence on DNA recruits Mediator

A plausible mechanism for Mediator recruitment is that TAs bind to DNA and, once present, they can directly or indirectly bind Mediator. Our observations are consistent with such a sequential model: at 50 nM Gal4-VP16^{649}, Mediator was over eight-fold more likely to occupy DNA during time points when Gal4-VP16^{649} was present as compared to intervals without Gal4-VP16^{649} (**Figure 2D**). To rule out non-sequential alternative mechanisms (e.g., those in which TA binds before Mediator simply because TA generally binds to DNA faster than Mediator), binding time courses for 100 randomly selected DNA molecules from the 10 nM (**Figure 2E**) and 50 nM (**Figure 2F**) Gal4-VP16^{649} data sets were plotted as two-color rastergrams. Sorting by time of initial Gal4-VP16^{649} binding (left panels) shows that intervals with one or more Mediator complexes present (blue and green horizontal lines) were more frequent and longer-lived after initial TA binding than before. In contrast, when the same 100 DNA molecules were sorted by the time of initial Med7^{549}

binding (**Figure 2E, F**, right, black points), TA binding intervals (e.g., **Figure 2E, F**, right, red or blue horizontal lines) were almost equally dense before and after the first Mediator binding. Furthermore, the subset of DNAs that never bound TA (**Figure 2E**, left, DNA molecule numbers 71 – 100) almost never bound Mediator. The rare Mediator binding observed in the absence of fluorescent TA can be largely explained by dark TA dimers caused by photobleaching or the small fraction of incompletely labeled molecules (**Figure S3A**; see Methods) and nonspecific binding. Thus, our observations support the sequential model in which TA must bind first and remain present on the DNA for Mediator to bind.

Mediator is recruited to UAS but stabilized by core promoter

Previous reports show Mediator interacting with TAs at the UAS[27,31,58–60]; or binding directly to the PIC at a core promoter[36,38,60,61]. To examine which of these interactions occur in our system, Mediator binding to the UAS+promoter DNA was compared to "UAS-only" or "Promoter-only" constructs lacking one or the other of these elements (**Table S4**). Two DNA constructs were sequentially attached to the same microscope slide to ensure identical conditions, and then incubated with Med7^{549} YNE supplemented with 190 nM unlabeled Gal4-VP16^{50} in the absence of NTPs. Mediator binding was equally fast and extensive at UAS+promoter DNA and UAS-only DNA locations, with more than half of DNAs displaying initial Mediator binding within the first 500 s (**Figure 3A, B**). In contrast, Mediator binding to UAS+promoter and Promoter-only (which differ only by having the Gal4 binding

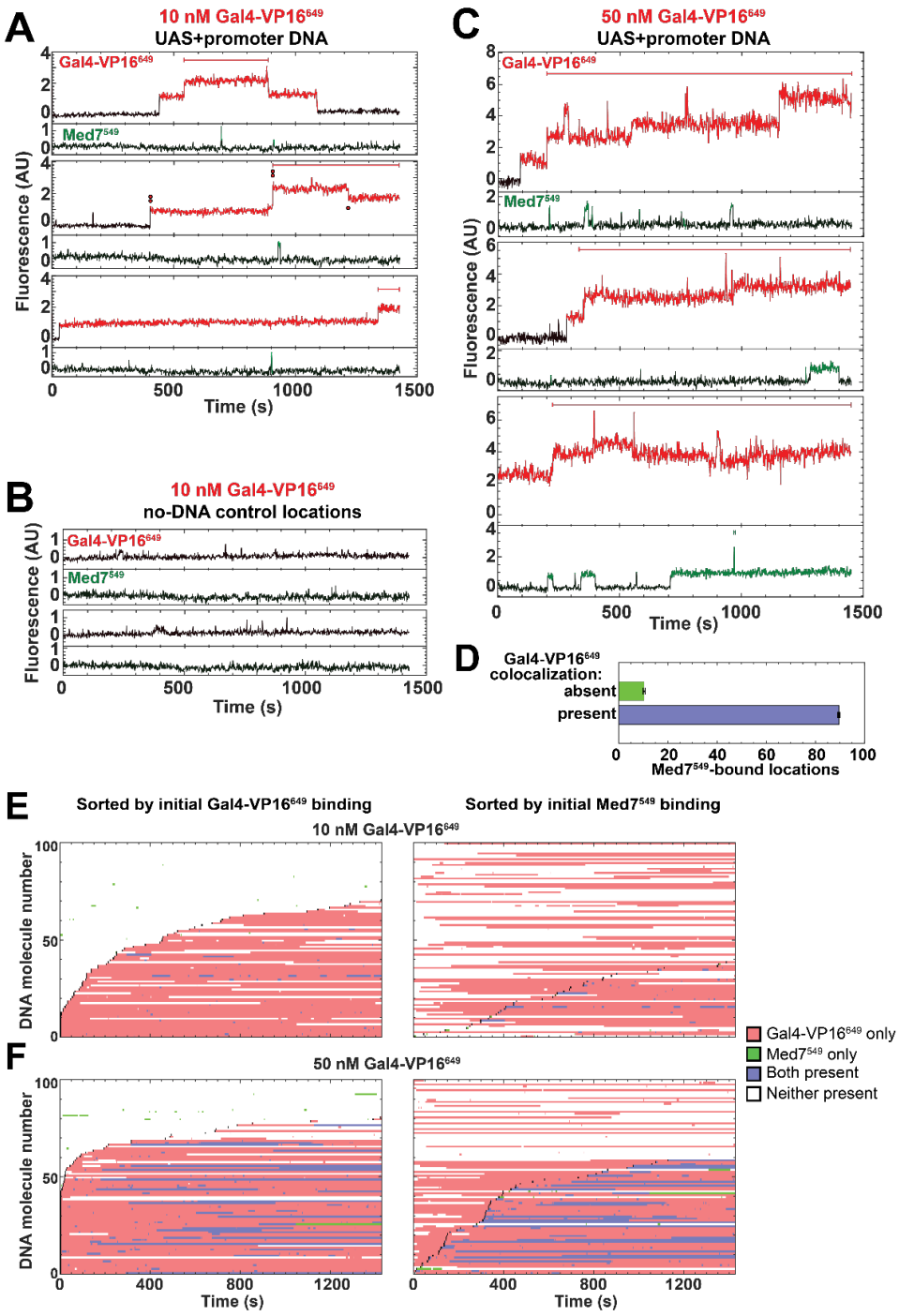

Figure 2: TA-dependent recruitment of Mediator to a transcription template DNA. (A) Example Gal4-VP16^{649} (red) and Med7^{549} (green) fluorescence intensity time records from the locations of three individual DNA molecules in the presence of YNE plus 10 nM Gal4-VP16^{649}. Color: time points at which a fluorescent spot was detected[46,47]. Horizontal bars: time intervals in which more than one molecule was simultaneously present. Step changes in Gal4-VP16^{649} fluorescence intensity are presumed to correspond to arrival or departure of dimers with either one (single dot) or two (two dots) dye molecules. **(B)** Intensity records from two control no-DNA locations in the same experiment as (A). **(C)** Same as (A), but with 50 nM Gal4-VP16^{649}. **(D)** Time-averaged fraction (± S.E.) of Mediator-bound DNA locations that either do (blue) or do not (green) have one or more Gal4-VP16^{649} molecules bound. Data are from the experiment in (C); from N_{DNA} = 637 DNA molecules and N_t = 1,024 time points per molecule. **(E)** Rastergram plots from 100 randomly selected DNA molecules from the experiment in (A). Each horizontal line displays the time record for a single DNA location, color coded to indicate Gal4-VP16^{649} and Med7^{549} presence. In the left and right plots, the same DNA molecules are ordered by the time of first Gal4-VP16^{649} binding or time of first Med7^{549} binding, respectively. The start of each first binding event is marked (black). **(F)** Same as (E), but from the 50 nM Gal4-VP16^{649} experiment in (C).

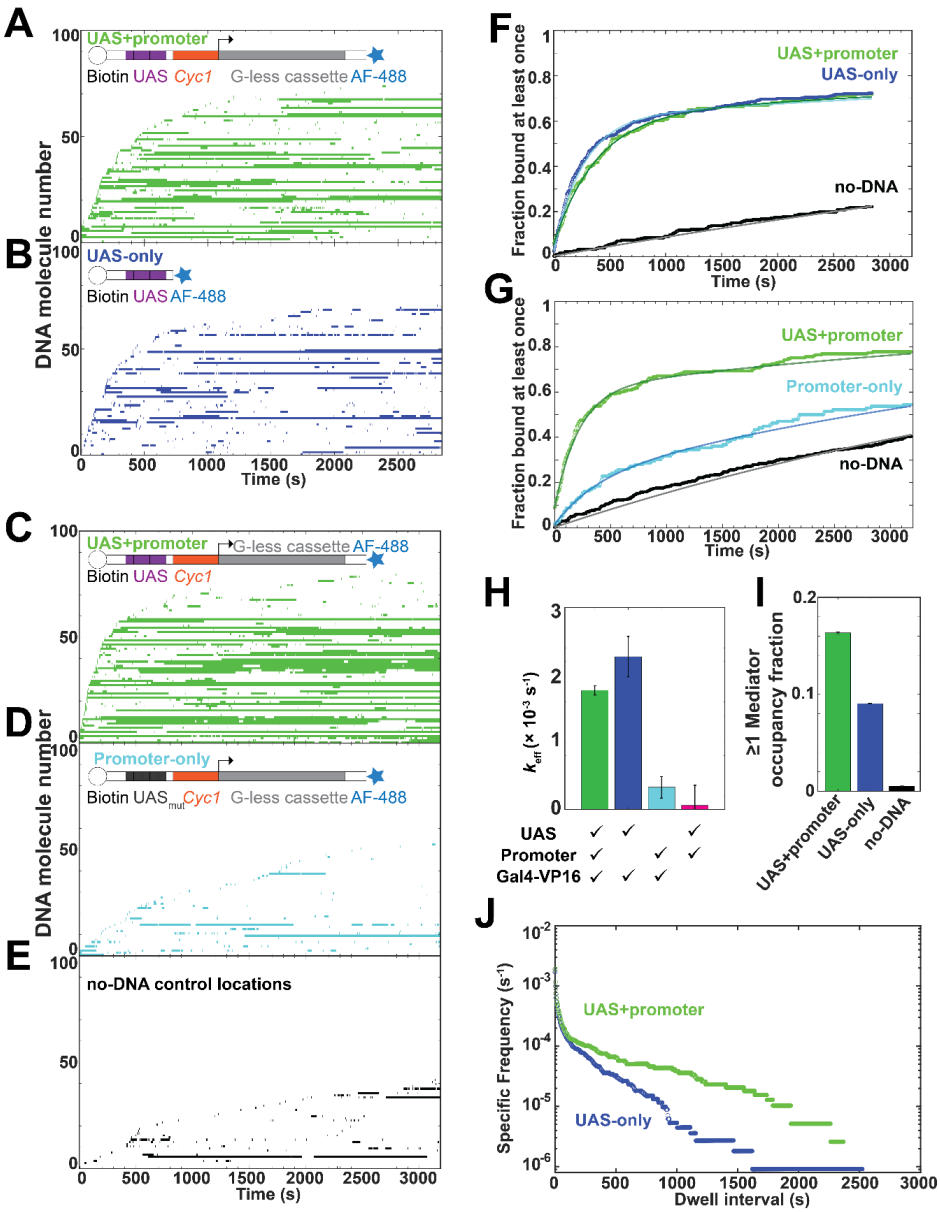

Figure 3: Mediator association strongly depends on UAS and activator, but not core promoter. Single-molecule experiments were conducted using 190 nM unlabeled Gal4-VP16. **(A, B)** Rastergrams for Med7^{549} binding in an experiment in which UAS+promoter DNA (A) and UAS-only DNA (in which the DNA was truncated following the UAS, B) were tethered at known locations in the same sample (see Methods). Each plot shows data from 100 randomly selected DNA locations, sorted by the time of initial Med7^{549} arrival. Colored bars indicate times during which one or more Med7^{549} molecules were bound. **(C, D)** Same as (A,B) but from an experiment which simultaneously monitored UAS+promoter (C) and promoter-only (in which the Gal4 binding sequences were ablated, D) DNA. **(E)** Data from control no-DNA location from the same experiment as (C, D). The no-DNA control from the experiment in (A, B) shows even less binding (**Table S2**). **(F)** Cumulative fraction of UAS+promoter and UAS-only DNA bound by at least one Med7^{549} molecule as a function of time from addition of extract, from the experiment in (A,B). Lines are fits (see **Table S2**) to an exponential specific-binding model that accounts for the contribution of non-specific surface binding[47]. **(G)** Same as (F), except using data from the experiment in (C-E). **(H)** Effective first-order DNA-specific association rate constants k_{eff} (± S.E.) for Med7^{549} measured for different DNAs in the presence of zero or 190 nM Gal4-VP16. Data are weighted averages of values from multiple replicates (**Table S2**). **(I)** Fraction of time (± S.E.) in which UAS+promoter and UAS-only DNAs were bound by at least one Mediator in the experiment shown in (A, B, F). Number of observations given in **Table S2**. **(J)** Cumulative distributions of DNA-specific Med7^{549} dwell times on UAS+promoter and UAS-only DNA in the experiment shown in (A, B). Each continuous time interval with ≥1 labeled Med7^{549} molecules present was scored as a single dwell. Specific frequency values were calculated by correcting for the contribution of non-specific surface binding measured at no-DNA locations (panel F, black curve).

sites mutated in the latter) showed much less extensive binding to the Promoter-only DNA (**Figure 3C, D**). Indeed, binding at Promoter-only DNA locations resembled that at control no-DNA locations (**Figure 3E**), suggesting that most of the observed binding at Promoter-only locations was due to non-specific Mediator binding to the slide surface. Non-specific Mediator binding was higher at 190 nM Gal4-VP16 than at the 50 nM Gal4-VP16^{649} used earlier (compare **Figure 3E** to **Figure S2B**).

To quantitatively compare binding on the different DNA constructs, effective DNA-specific Mediator association rate constants (k_{eff}, which correct for an observed slow inactivation or departure of the DNA molecules in YNE; see Methods and **Figure S4D**) were calculated using the distributions of time intervals before initial binding of Mediator observed at each DNA location and no-DNA control location[47] (**Figure 3F**, **G**). The k_{eff} values for UAS+promoter and UAS-only DNA were identical within experimental uncertainty (**Figure 3F** and **H**, compare green and blue), suggesting that initial Mediator binding is primarily to TAs at the UAS. In agreement, DNA-specific Mediator association is essentially absent without Gal4-VP16 (**Figure 3H**, magenta; **Figure S4A-C**). Importantly, the low rate of DNA-specific Mediator binding to Promoter-only DNA suggests UAS-independent binding of Mediator to the core promoter makes little contribution to overall Mediator association kinetics (**Figure 3H,** compare cyan to green; **Table S2**).

Mediator association kinetics were essentially identical on the UAS+promoter and UAS-only DNAs (**Figure 3F, H**). However, the fraction of time with Mediator present was substantially higher on UAS+promoter DNA (**Figure 3I**), largely due to longer average Mediator dwell times on UAS+promoter DNA (**Figure 3J**). Specifically, the dwell

time distributions when fit to models with three components (**Figure S4E**), showed the longest component significantly lengthened by the presence of the core promoter (compare τ_L values in **Figure S4F**). In previous experiments (also conducted, as here, in the absence of NTPs) we observed similar recruitment to TAs at the UAS but kinetic stabilization by core promoter for RNApII and TFIIF[49]. We propose that Mediator, RNApII, TFIIF, and possibly other coactivators and general transcription factors[49,50,62] assemble relatively short-lived pre-PICs while tethered to TAs at the UAS, which then transfer to core promoter sequences to form PICs, which in the absence of NTPs can last for hundreds of seconds[49,59].

Mediator recruits RNApII to the template

The proposed model predicts that the pre-PIC contains both Mediator and RNApII. To investigate the pathway(s) by which these components are assembled into the pre-PIC, we analyzed CoSMoS data from fluorescently labeled Mediator (Med7^{549}) and RNApII (Rpb1^{Cy5}) YNE supplemented with 190 nM unlabeled Gal4-VP16 in the absence of NTPs (**Figure 4**). Like Mediator, Rpb1^{Cy5} bound primarily at DNA locations, with little non-specific binding at no-DNA sites (**Figure S5A-B).** Most commonly, RNApII molecules arrived at DNA molecules where Mediator was already present (e.g., start of each purple-shaded dwell in **Figure 4A**). RNApII arrival on DNA lacking Mediator was rare (e.g., **Figure 4A**, orange; and **Figure 4B**, left, few red lines above the black curve), and these rare Mediator-independent interactions often had short dwell times similar to RNApII bound nonspecifically to the slide surface (**Figure S5B)**[50]. Mediator arrival on the DNA generally preceded RNApII arrival (**Figure 4B**, right, many green lines above the black curve), and Mediator could bind to DNAs that never recruited RNApII (**Figure 4B**, DNA molecules 44-100). At these high TA concentrations, we observed occasions where two or more Med7^{549} (**Figure 4A**, green bars), and less frequently, two or more Rpb1^{Cy5} (**Figure 4A**, red bars) molecules were present on the same DNA. Multiple simultaneously bound RNApII molecules were virtually exclusively observed at DNAs with more than one Mediator molecule. Taken together, these observations support the proposal that Mediator recruits RNApII in the formation

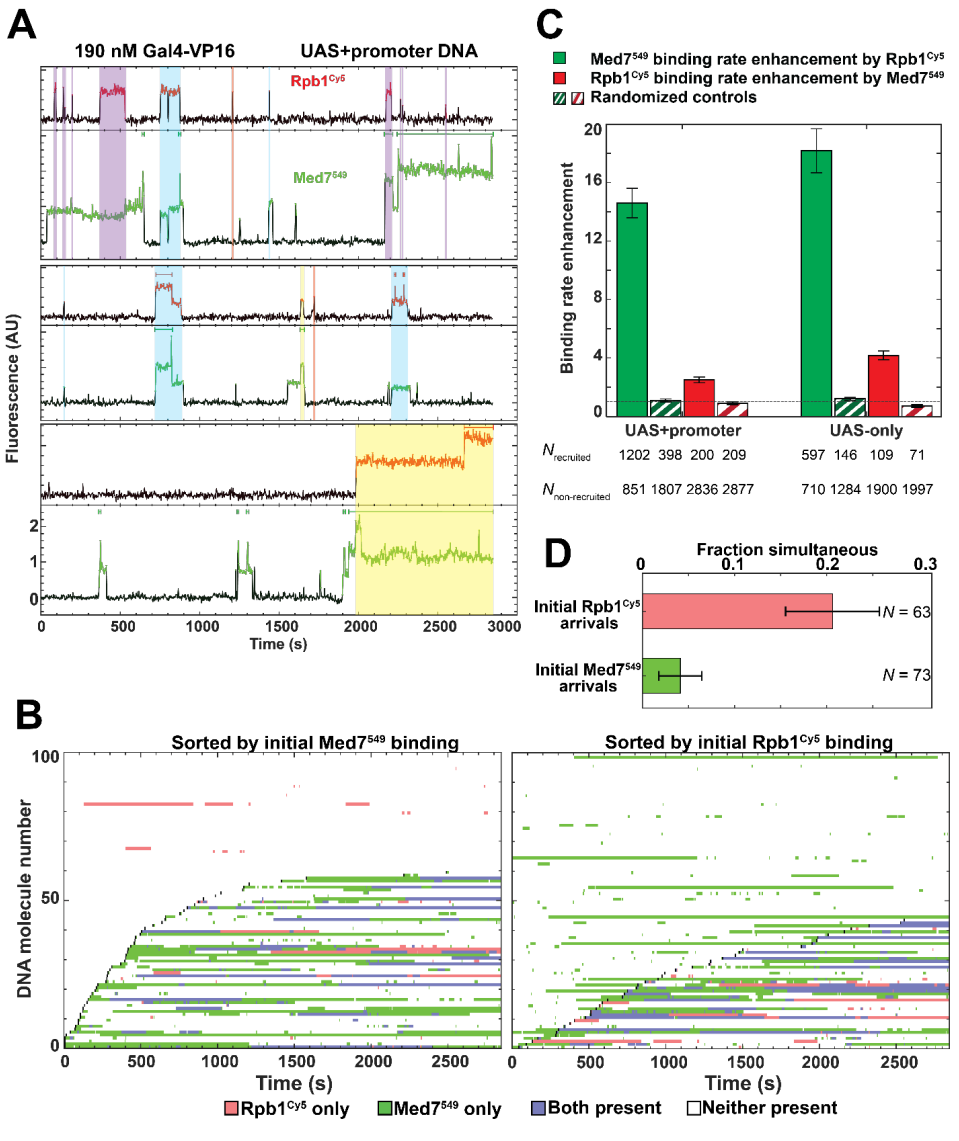

Figure 4: RNApII recruitment by Mediator during activator-dependent PIC assembly. (A) Example Rpb1^{Cy5} (red) and Med7^{549} (green) fluorescence intensity time records recorded from the locations of three individual UAS+promoter DNA molecules in YNE plus 190 nM Gal4- VP16 (from same experiment as **Figure 2A)**. Red and green colors indicate times at which a fluorescent spot was detected. Red and green bars mark simultaneous presence of more than one Rpb1^{Cy5} or Med7^{549}, respectively. Shading highlights RNApII-bound intervals in which RNApII arrived when Mediator was already present (purple), when both RNApII and Mediator arrived simultaneously (blue), and when RNApII arrived while no Mediator was detected (orange). Yellow shading represents the rarely observed cases in which Mediator was present before RNApII arrived simultaneously with a second Mediator molecule. **(B)** Rastergrams, plotted as in **Figure 2E** and **F**, for 100 randomly selected DNA molecules from the experiment in (A). **(C)** Fold increase (± S.E.) in Rpb1^{Cy5} binding frequency to DNA molecules when Med7^{549} was present relative to when it was absent (green) and fold increase in Med7^{549} binding to a DNA when Rpb1^{Cy5} was present relative to when it was absent (red). A binding rate enhancement of one (horizontal dashed line) indicates no preference. **(D)** Simultaneous arrival of the initial molecules of Mediator and RNApII to 100 randomly selected DNA locations. *Red*, bars indicate the fraction of the initial Rpb1^{Cy5} arrivals on each DNA that appeared simultaneous (within ± 2.7 s) with the arrival of Med7^{549} at the same DNA. *Green*, fraction of the initial Med7^{549} arrivals that appeared simultaneous with the arrival of Rpb1^{Cy5}.

of UAS-bound pre-PICs, presumably for rapid transfer to the core promoter during activated transcription[49].

To quantitate the apparent dependence of RNApII recruitment on Mediator, we calculated the effect of DNA-bound Mediator on RNApII association frequency to DNA. RNApII molecules bound to Mediator-occupied UAS+promoter DNA >14-fold more frequently than to DNA molecules with no Mediator present (**Figure 4C**, left, green). This high "binding rate enhancement" was not simply caused by Mediator binding more rapidly than RNApII: a control analysis randomly pairing Mediator and RNApII records (**Figure 4C**, left, green striped bar) showed no enhancement, as expected for independent events. Enhancement of Mediator binding rate to DNAs with RNApII already present compared to those without was considerably smaller (**Figure 4C**, red bars), but still greater than the randomized control value of ~1 (**Figure 4C**, red striped bars). We attribute this small effect to occasional Med7^{549} fluorescence blinking and/or photobleaching rather than RNApII recruiting Mediator to DNA. Importantly, binding rate enhancements on UAS-only DNA (**Figure 4C**, right, green) were similar to those on UAS+promoter DNA, consistent with both Mediator (**Figure 3**) and RNApII being initially recruited directly to the UAS-bound TAs[49].

Mediator and RNApII can arrive at DNA in a pre-formed complex

While Mediator most often preceded RNApII on DNA, simultaneous arrivals were also frequently seen (e.g., **Figure 4A**, starts of blue and yellow intervals). Approximately 20% of initial Rpb1^{Cy5} arrivals on each DNA were simultaneous with Med7^{549} arrivals (**Figure 4D**). The simultaneous arrivals were not coincidences: random time-offset control analyses exhibited zero simultaneous arrivals on 100 DNAs analyzed (see Methods). In contrast only ~5% of initial Mediator arrivals were accompanied by simultaneous Rpb1^{Cy5} arrivals. This is expected, as Mediator arrivals greatly outnumber RNApII arrivals (**Figure 4B**).

In a complementary analysis, we examined the formation of each Mediator/RNApII/DNA ternary complex. As expected, the distribution of time intervals between Mediator arrival and RNApII arrival ($t^{\mathrm{arr}}_{\mathrm{RNApII}} - t^{\mathrm{arr}}_{\mathrm{Med}}$; **Figure S5C**) showed that the majority of ternary complexes were formed with Mediator arriving prior to RNApII (**Figure S5C**, green bars). As before, roughly one-fifth of the ternary complexes were formed by Mediator and RNApII arriving simultaneously (**Figure S5C**, blue). Additionally, kinetic analysis confirms that the apparently simultaneous arrivals cannot be accounted for by sequential arrival of the two proteins within the ± 2.7 s time resolution of the experiment (**Figure S5C**, compare blue bars to curves). Consistent with our conclusions that Mediator (**Figure 3**) and RNApII[49] are initially recruited to the UAS, results obtained with UAS-only were essentially identical to UAS+promoter DNA (**Figure S5D**). Thus, the data suggest that pre-formed protein complexes that contain both Mediator and RNApII are present in YNE and account for a significant fraction of the RNApII recruitment to the UAS. This fraction may be even higher in cells since nucleoplasm is more concentrated than YNE and the higher concentrations may drive association of protein complexes.

Mediator tethers RNApII to UAS-bound activator

Mediator can arrive at the TA-occupied UAS independently of RNApII, whereas RNApII arrival usually had simultaneous or prior Mediator arrival. The inverse pattern was seen with protein departures (compare **Figure S5C-D** with **E-F**). Most commonly, RNApII dissociated from the UAS before Mediator. The second most common category of events were those in which the two departed simultaneously. Only rarely did Mediator depart first. The arrival and departure data together are consistent with Mediator being able to function as a physical tether between UAS-bound TAs and RNApII. The fact that Mediator can remain bound after RNApII dissociation raises the possibility that a single Mediator binding event at the UAS could promote multiple rounds of transcription.

Mediator occupancy is increased synergistically by multiple activator molecules

In the simplest model for TA-Mediator interactions, one TA molecule would recruit one Mediator complex. However, we noted far less Mediator occupancy in the 10 nM TA experiment than at 50 nM TA, even when a similar fraction of DNAs were occupied by TA (compare **Figures 2E and F**). We suspected this was related to multiple TAs being able to bind the five Gal4 sites in the UAS. Activator synergy in stimulation of RNApII transcription is well-documented in vivo, but can be explained by many different models (see Discussion)[9,11,12,14,16–19]. We therefore investigated whether cooperative recruitment of Mediator by multiple activators was occurring in our system.

To quantitate the number of TA and Mediator molecules on each DNA, the Bayesian machine learning program *tapqir* (see Methods)[63] was used to determine spot fluorescence intensities, which can serve as a proxy for protein stoichiometry. Data from four different TA concentration experiments were analyzed (although note that unlabeled TA was

used for the 190 nM experiment, as background fluorescence is too high at this concentration of labeled protein). At late time points in each experiment (~1,000 s or more), individual TA and Mediator molecules were still arriving at and departing from DNA (**Figures 2-4**). However, the mean fluorescence intensities of Gal4-VP16^{649} and Med7^{549} spots (**Figure S6A** and **B**, respectively) plateaued, suggesting the reactions (which do not contain NTPs) had reached equilibrium. Consistent with this interpretation, the time required to reach the equilibrium plateau shortened with increasing TA concentrations. We computed the mean number of Gal4-VP16 dimers bound during this plateau by combining the fractions of DNAs occupied by at least one Gal4-VP16^{649} (**Figure S6C,** red), the fits to the Gal4-VP16^{649} fluorescence intensity distributions at those DNA molecules, (e.g., **Figure S3B**; **Supplementary data file 1**), and a correction for the fraction of unlabeled Gal4-VP16 monomers (see Methods). An analogous calculation was done for Mediator data. Gal4-VP16^{649} mean occupancy fraction (**Figure S6C**, red) increased roughly hyperbolically with concentration. Similarly, the mean number of TA molecules per DNA (**Figure 5A**, red) was well fit by a hyperbolic binding curve (Hill coefficient of 1), consistent with a simple independent binding model. Strikingly, Med7^{549} occupancy fraction (**Figure S6C**, green) and mean number of Mediator molecules per DNA (**Figure 5A**, green) exhibited a sigmoidal relationship with Gal4-VP16 concentration, increasing very little from 10 to 25 nM activator but showing a marked increase from 25 to 190 nM activator. The fit of the mean number of Mediator molecules per DNA to the Hill equation was best at a Hill coefficient of 2.9 (**Figure 5A**), consistent with switch-like or cooperative response to TA concentration.

A likely possible explanation for the non-linear response of Mediator to TA is that DNA molecules carrying only a single TA dimer have a relatively weak interaction with Mediator; while two or more TA present on the DNA can bind Mediator more strongly. To determine the relative stoichiometry of TA to Mediator (which was predominantly present at one molecule per template; e.g., **Figure 2C**), we plotted distributions of Gal4-VP16^{649} fluorescence intensities when Mediator was absent (**Figure 5B**, red points) or present (**Figure 5B**, blue points). Strikingly, the Gal4-VP16^{649} fluorescence intensity on DNA without Mediator most often corresponded to two dye molecules (i.e., one activator dimer; **Figure 5B**, red points). In contrast, when Mediator was present on a DNA there was a clear shift to a broader, multimodal distribution with mostly higher Gal4-VP16^{649} intensities corresponding to the presence of two or more TA dimers

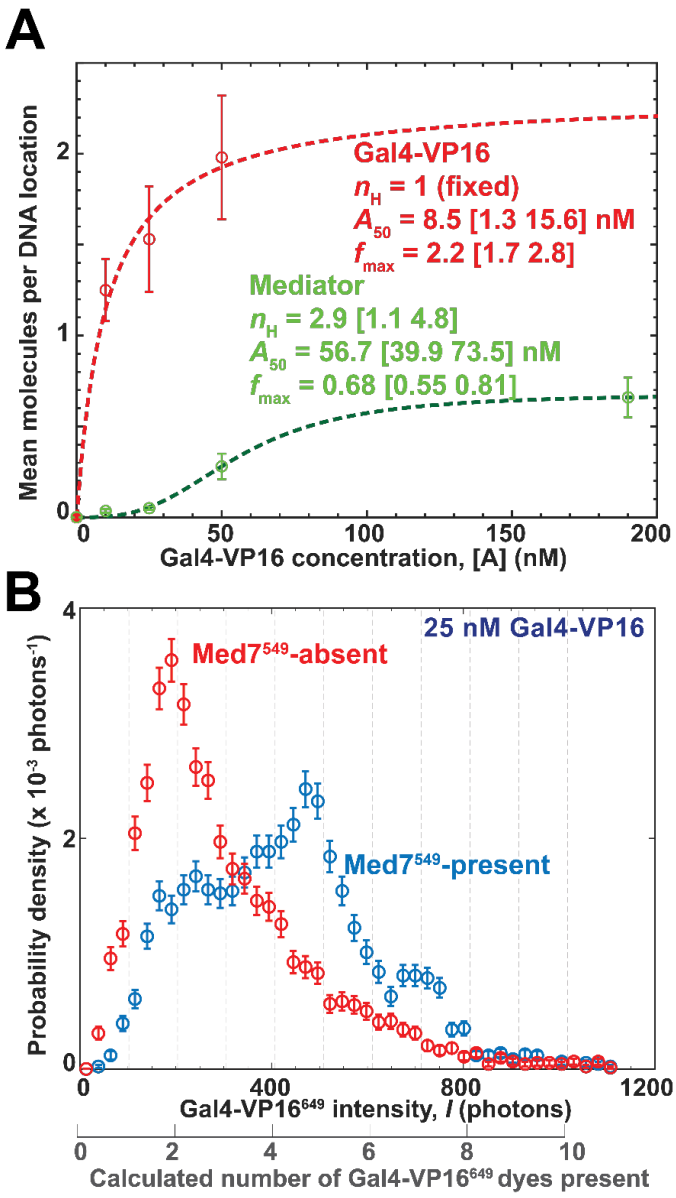

Figure 5: Mediator occupancy is cooperative with respect to TA concentration. (A) Mean (± S.E.) number of Gal4-VP16 and Mediator molecules per DNA at equilibrium (points; see Methods and **Table S3**) at different activator concentrations [A]. Data are from the 10 and 50 nM Gal4-VP16^{649} experiments in **Figure 2,** an additional experiment at 25 nM, and the 190 nM unlabeled Gal4-VP16 experiment in **Figure 3A**. Data at zero Gal4-VP16 are zero by definition (red point) and from the experiment in **Figure S4A** (green point). Gal4-VP16 (three [A] values) and Mediator (five [A] values) were **separately** fit to the Hill equation $f_{max}/[1+(A_{50}/[A])^{n_H}]$ (lines) yielding the indicated parameter values [68% C.I.]. f_{max} is the asymptotic value at high [A] and A_{50} is the [A] value producing a half-maximal value. The Hill coefficient, n_H was a variable parameter for the Mediator fit but was fixed at n_H = 1 for the activator fit. **(B)** Gal4-VP16^{649} equilibrium spot intensity distributions at DNA locations in the experiments at 25 nM Gal4-VP16^{649}. Intensity distributions (± S.E.; N_{DNA} = 620) are plotted for the 3,690 data points during which Med7^{549} was present (blue points) or for a randomly-selected, time-matched set of 3,960 points during which Med7^{549} was absent (red points). Intensities are expressed both as the number of photons emitted per frame and the calculated number of dyes present.

(**Figure 5B**, blue points). We conclude that a Mediator molecule preferentially associates with a DNA carrying two or more TA molecules.

Modeling of synergistic activator-Mediator interactions

To quantitatively explain the dependence of equilibrium TA and Mediator occupancies on the concentration of TA, we asked whether the TA and Mediator data, *taken together*, could distinguish between particular equilibrium binding mechanisms. (This is in contrast to the fits in **Figure 5A**, in which the TA and Mediator data were fit separately to simple phenomenological models.) We considered model mechanisms in which up to five TA molecules bind to DNA and at most one Mediator molecule per DNA can bind through activator-Mediator interaction(s). For simplicity, we treated all five possible activator-DNA contacts as having identical binding interfaces.

To start, we defined a "single-bridging" model (**Figure 6A**) that allows only a single interaction at a time between Mediator and the bound activators. Specifically, the model assumes that the TA dimers bind DNA independently and that the Mediator molecule binds through interaction with any single TA dimer. This model has only two variable parameters: K_a, the association equilibrium constant for a Gal4-VP16 dimer binding to a Gal4 binding site; and m, the strength of the Gal4-VP16—Mediator binding interaction expressed as a Boltzmann factor (see Methods). Computing the statistical weights associated with all molecular states in the model allowed us to calculate the parameter values that gave the best fit of the model to the equilibrium occupancy data for Gal4-VP16 and Mediator taken together (**Figure 6B**). The best fit failed to match the occupancy data, in particular failing to reproduce the sigmoidal shape of the Mediator occupancy curve (**Figure 6B**, inset), showing that this model is inconsistent with the data.

We then considered a single-bridging model in which neighboring DNA-bound TAs interact with each other (**Figure 6C**) as has been proposed for other activator/UAS combinations[64–67]. For simplicity, all the TA-TA contacts were assumed identical and the TA-TA

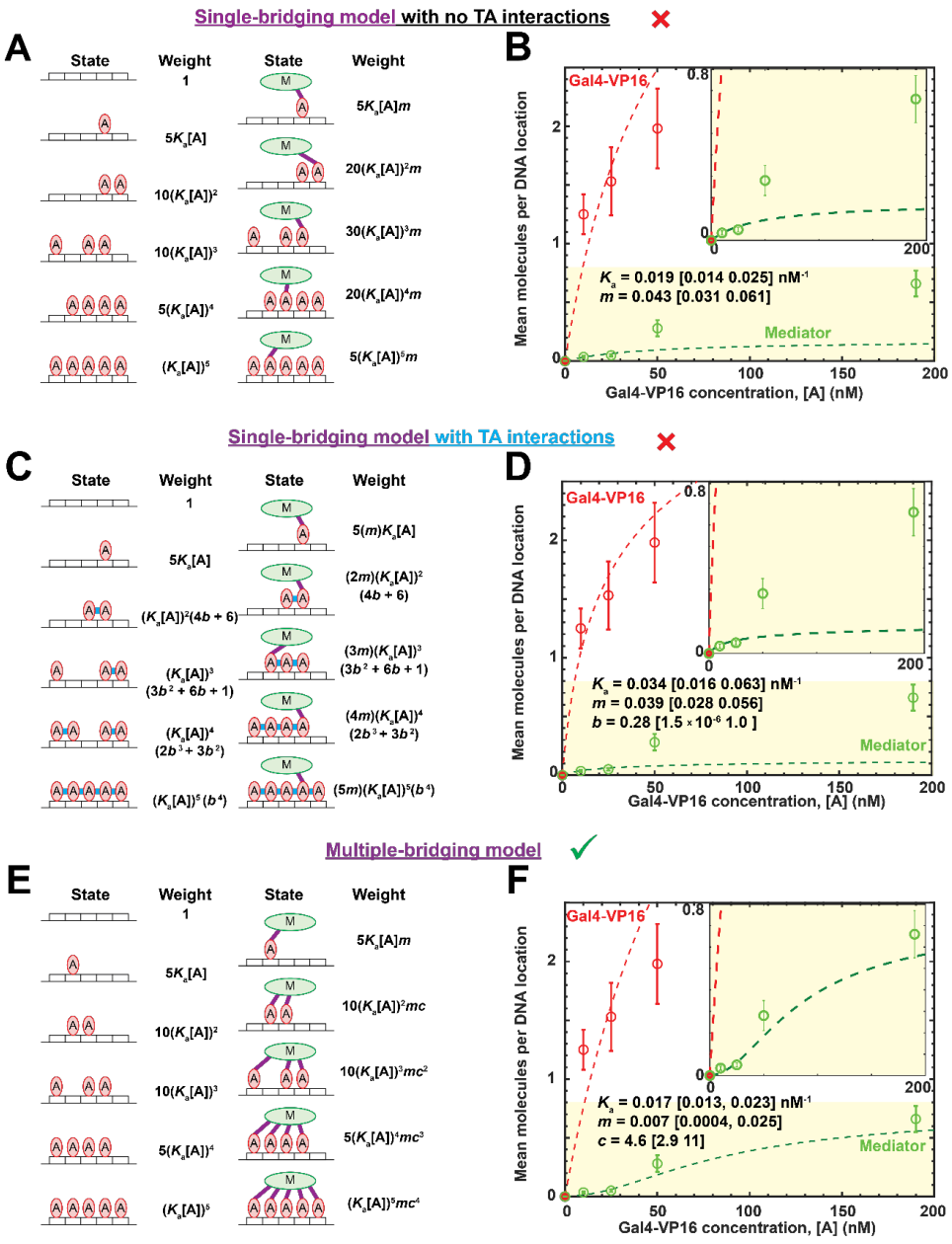

Figure 6: Statistical mechanical models and best fits for equilibrium TA and Mediator occupancy at the UAS. (A) States and statistical weights[17] defining the single-bridging equilibrium model for binding of Gal4-VP16 dimers (red) and Mediator (green) to a DNA with five Gal4 binding sites (white rectangles). In this model, states can include a maximum of one TA-Mediator interaction (purple lines) and no TA-TA interactions. Each cartoon illustrates only one of the possible molecular arrangements included in that state; the statistical weights account for all arrangements. The weights depend on two variable parameters (K_a and m; see text) and the TA concentration [A]. **(B)** Mean (± S.E.) number of Gal4-VP16 and Mediator molecules per DNA at equilibrium (points; same data as in **Figure 5A**). Lines are the best fit (relative likelihood $p_A = 2.06 \times 10^{-9}$) of the combined Gal4-VP16 and Mediator data to the model (A), yielding the indicated parameter values [90% CI]. **(C)** Same as (A) but for the "single-bridging with TA interactions" model ($p_C = 9.71 \times 10^{-9}$). The model is identical to that in (A) except that it adds direct interactions (with strength represented by Boltzmann factor b; see Methods) between adjacent TAs (blue lines). **(D)** Same data as in (B) with best fit to model in (C). **(E)** Same as (A), but for the "multiple-bridging" equilibrium model ($p_E = 2.75 \times 10^{-5}$). The model assumes that every DNA-bound TA bridges (purple) between DNA and Mediator when present but does not include direct TA-TA interactions. The weights have three variable parameters (K_a, m, and c; see text). **(F)** Same data as in (B) with best fit to model in (E). We favor the model in (E) (checkmark) over those in (A) and (C) (×); see text.

binding energy is represented by the Boltzmann factor *b*. Despite allowing this additional interaction between adjacent TAs, the best fit of this model to the equilibrium occupancy data for Gal4-VP16 and Mediator taken together again failed to reproduce the shape of the Mediator occupancy curve (**Figure 6D**) showing that this model too is inconsistent with the data.

Since neither of the above models gave good fits to the data, we considered the alternative simple "multiple-bridging" model shown in **Figure 6E**. This model lacks the direct TA-TA interactions of the model in **Figure 6C** but instead includes interactions between Mediator and all TAs present on the DNA when Mediator is present. The second through fifth TA−Mediator interactions are more favorable than the first because when forming these interactions Mediator is already in close proximity to the DNA-bound TAs, leading to a reduced entropic cost of interaction. For simplicity the second through fifth TA−Mediator interactions are each assumed to have the same Boltzmann factor, *c*, so that the multiple-bridging model contains the same number of variable parameters as the single-bridging model with TA interactions. The multiple-bridging model fits the equilibrium occupancy data for Gal4-VP16 and Mediator better than the single-bridging model with TA interactions (likelihood ratio $p_E / p_C = 2.83 \times 10^3$). Unlike the latter, the best fit of the multiple-bridging model was in reasonable agreement with the data across all activator concentrations, reproducing the higher binding of Gal4-VP16 than Mediator, the roughly hyperbolic activator binding curve, and the sigmoidal Mediator binding curve (**Figure 6F**). Furthermore, the parameter values produced by the fit were roughly those expected in the cases in which there are prior measurements of the interaction strengths (see Methods). Thus, the observed binding curves can be quantitatively accounted for by a simple three-parameter model based on multiple TAs bridging between DNA and Mediator. This analysis only evaluates the agreement between this simple model and the data; more complex models including additional interactions and/or parameters might better fit the data. In contrast, the simple single-bridging models were inconsistent with the data irrespective of whether they did not (**Figure 6B**) or did (**Figure 6D**) include interactions between neighboring activators.

Discussion

Here we image the Gal4-VP16 activator, Mediator, and RNApII in the context of nuclear extract using single-molecule microscopy. While consistent with previous genomic and structural studies[39,62,68,69], our results provide important new insights about factor dynamics, which are inaccessible using these other methods. The interactions between factors allow for multiple routes to PIC formation, but real time monitoring of events on individual DNA templates reveals which pathways predominate (**Figure 7**, blue shading). Our experiments also reveal a mechanism by which multiple TAs can synergistically activate gene expression.

Hierarchical interactions recruit Mediator and RNApII to the UAS

Cryo-EM structures of the PIC or initially transcribing complex (ITC) show Mediator interacting with GTFs and RNApII at the core promoter[35–37,39,70–72]. Temperature sensitive mutants indicate that Mediator is important for PIC assembly and stabilization in vivo[61]. However, ChIP-seq data show Mediator crosslinking to enhancer/UAS regions, usually to a greater extent than at core promoters, consistent with Mediator binding to UAS-associated TAs. These distinct configurations are often thought to happen simultaneously, with Mediator creating a DNA loop between UAS-associated TAs and the RNApII-containing PIC on the promoter.

Our single-molecule experiments suggest a different model in which TA-tethered Mediator nucleates assembly of a pre-PIC comprised of RNApII and a subset of GTFs. Initial binding of Mediator to DNA was primarily at the UAS, not the core promoter (**Figure 3**), and dependent on the presence of one (**Figure 7**, steps *i, ii*) or more (**Figure 7**, steps *iii, iv*) activator molecules on the UAS (**Figures 2, 3, S4**). This behavior mirrors initial binding of RNApII and TFIIF, which we showed also occurs at the UAS rather than the core promoter[49]. DNA molecules with multiple activator molecules showed faster Mediator association, longer Mediator dwells, and sometimes accumulated multiple copies of Mediator (**Figures 2A, C** and **4A**).

Imaging of Mediator and RNApII together showed that Mediator presence was required for RNApII binding to a DNA molecule (**Figure 4C**). While often modeled arriving as a pre-formed complex, we observed (**Figure 4D, S5C, D**) that Mediator most often arrived at the UAS before RNApII (**Figure 7**, step *vi*), and only sometimes together (**Figure 7**, step *vii*). There were also many Mediator binding events where RNApII never appeared, but not the converse (**Figure 4B**). In the absence of NTPs, RNApII predominantly left the DNA before or simultaneously with Mediator (**Figure S5E, F**). Therefore, RNApII-induced conformation changes in Mediator[68] are not required for delivery to the UAS. "Empty" Mediator can bind to UAS-associated TAs and then wait at the UAS to recruit RNApII.

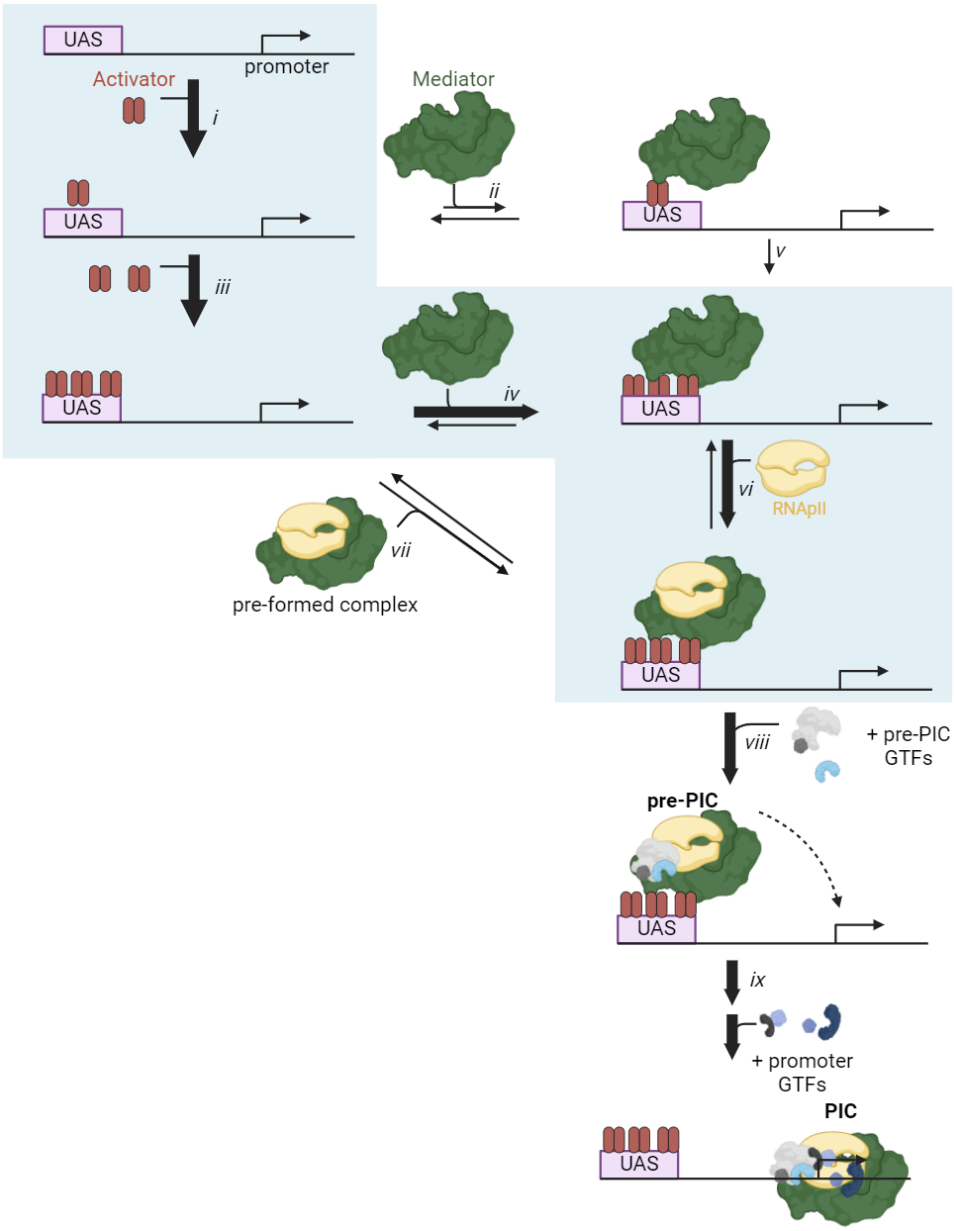

Figure 7: Pathway of Mediator and RNApII recruitment during activator-dependent PIC assembly. Our single-molecule experiments reveal hierarchical recruitment of activator, Mediator, and RNApII (depicted in red, green, and yellow, respectively) at the UAS. The most commonly observed pathway for the formation of a UAS-bound pre-PIC is shaded in blue. Recruitment of Mediator to the UAS is cooperative with respect to activator concentration, likely because multiple activator dimers can bridge between DNA and a single Mediator.

Nonetheless, we observed up to a third of RNApII arrivals were simultaneous with Mediator, and roughly half were simultaneous with TFIIF[49]. These numbers are consistent with estimates of RNApII-Mediator and RNApII-TFIIF complexes derived from co-immunoprecipitation from extracts, although that study concluded that there was little or no trimer complex with all three factors[73]. Preformed complexes might be more common in vivo, where factor concentrations are likely higher. These off-DNA interactions likely account for previously reported RNApII "holoenzymes", which had varying GTF content depending on isolation method, but characteristically contained RNApII, Mediator, and TFIIF[6,74–76].

Mediator pre-PICs likely transfer from UAS to core promoter

Our pre-PIC model is strongly supported by a recent structure (designated the Med-PIC^{early} complex) showing Gal4-VP16 tethering Mediator, RNApII, TFIIF, and TFIIB at the UAS[40]. Although the intrinsically disordered VP16 TAD and Med15 Activator Binding Domains (ABDs) were not resolved, this structure is consistent with demonstrated contacts between activator TADs and Mediator tail subunits[30,77,78]. These tail module interactions are important for Mediator recruitment to promoters in vivo[32,79,80], although the universality of these interactions has been disputed[28].

Our model further proposes a physical transfer of the pre-PIC from UAS to the core promoter (**Figure 7**, step *ix*), where TATA-binding protein is presumably required to receive the complex. Upon completion of the PIC, progression to initiation is likely rapid. While transfer has not yet been directly demonstrated, several observations support this model. In the absence of NTPs to prevent transcription initiation, we see an increase in long Mediator dwell times on UAS+promoter versus UAS only DNAs (**Figure 3J**, **Figure S4E-F**), as previously observed for RNApII and TFIIF[49]. These extended dwells likely represent PICs, as they are greatly reduced by NTPs. Our results parallel in vivo ChIP experiments showing that depletion of the TFIIH kinase, needed to trigger release of Mediator from the PIC, leads to strong increase of Mediator crosslinking at the core promoter[32,59,80,81].

A multiple-bridging model for activator synergy in Mediator recruitment

Transcription synergy occurs when multiple activator binding sites produce a gene output greater than the sum of the outputs driven by the individual sites[7,10,19,54]. Synergy is significant because it can produce non-linear, switch-like responses to TA concentration and can facilitate accurate

combinatorial gene regulation by multiple TAs. A wide variety of mechanisms have been proposed to explain synergy[12,18]. One classic mechanism for synergy is cooperative binding of TAs at adjacent DNA sites, which has been experimentally observed for several prokaryotic and eukaryotic TFs[54,64–67,82]. Another type of model is "kinetic synergy", where different activators act at distinct rate-limiting steps[9]. For example, one TA could be needed for relieving chromatin repression while the second accelerates PIC assembly directly.

Our experiments suggest a different TA synergy mechanism in Mediator recruitment, independent of cooperative TA binding or chromatin. First, the average number of Mediator molecules bound to DNA increased much more sharply than the number of TA molecules as TA concentration increased from 10 to 50 nM (**Figure 5A**). Second, individual DNA molecules with Mediator present were much more likely to have multiple bound activator molecules than DNAs without Mediator in the same experiment (**Figure 5B**). The data are inconsistent with the analyzed single-bridging mechanisms where Mediator interacts with only one TA molecule at a time, whether or not interactions occur between TA molecules at adjacent binding sites (**Figure 6A-D**). Instead, the data are consistent with a multiple-bridging model in which UAS-bound activators do not directly interact with each other, but two or more DNA-bound activators can simultaneously interact with the same Mediator (**Figure 6E, F**). During early work on activators, a generic multiple-bridging model with a single unidentified target was proposed to explain observations of synergy without TA cooperativity[10,19], and our results show that the Mediator is likely such a target.

Our multiple-bridging model is consistent with data suggesting multiple TAD interaction sites within a single Mediator[83], either via multiple Mediator subunits or perhaps even within a single Med15 subunit[24]. Multiple intrinsically disordered activator-binding domains (ABDs) are available to make dynamic, low affinity interactions with TADs[30,83,84]. Interestingly, recent in vivo imaging also suggests that the mammalian p300 histone acetyltransferase also requires at least two activator interactions for effective recruiting to chromatin[85]. Our data do not exclude the additional possibility that some TAD-Mediator interactions might be indirect (e.g., bridging through RNApII, GTFs, or other proteins).

A single template DNA can simultaneously associate with multiple Mediators and RNApII molecules (**Figure 4A** and ref. 49). Thus, a group of TAs at the UAS can likely assemble multiple pre-PICs, positioning them for rapid transfer to the promoter and transcript initiation. Pre-PIC formation at enhancers could be one mechanism for the clustering of activators and Mediator seen by live cell imaging, independent of any phase separation phenomena. We see no evidence for formation of large-scale liquid-like condensates in our extract system – Gal4-VP16, Mediator, and RNApII associate with the DNA in single-molecule steps[49,50] – but such mechanisms could provide further concentration of pre-PIC factors poised for transfer to promoters.

A multiple-bridging mechanism for Mediator recruitment by activators provides several potential advantages. First, it creates a straightforward mechanism for combinatorial regulation by multiple different activators binding to the same UAS, allowing more distinct transcription patterns. Even the simple compact promoters found in yeast often contain multiple TA binding sites, as illustrated by analyses of *HIS4*[86], *CYC1*[87], and *PHO5*[88]. Synergistic binding to multiple TAs also reduces the likelihood that Mediator can be "squelched" by non-productive interactions with single activators molecules in the nucleoplasm. Supporting this idea, purified Mediator showed stable binding to DNA with multiple activators, even in the presence of a large excess of free activator molecules in solution[83]. Finally, in vivo imaging of Gal4 show that a UAS with multiple binding sites allows for transcription bursts lasting beyond the time scale of individual Gal4 dwell times[89].

Our single-molecule studies provide important new insights into the dynamics of transcription activation using a simple extract system. Predictions of the TA:pre-PIC multi-bridging model can now be tested in more complex in vitro and in vivo systems. Even with additional complexities such as chromatin, multiple enhancers, and long-distance enhancer-promoter communication, we anticipate that single-molecule experiments and statistical mechanical analyses will provide further insight into the biochemical mechanisms of activation.

Limitations

Our single-molecule studies provide new insight into the pathways of activated transcription but come with limitations. One limitation is the ability to visualize only a subset of proteins (i.e., the ones that are fluorescently labeled) in each experiment. Investigating the participation of other proteins or protein complexes in the phenomena studied requires additional experiments in which those proteins are labeled. Though yeast nuclear extract approximates the protein composition inside the nucleus of a living cell, the extracts are more dilute than the nucleus, leading to possible

underestimation of the prevalence of protein-protein interactions. Finally, our statistical mechanical models are minimal models consistent with the data; this work does not exclude the possibility that more complex models might better explain the data.

Methods

Purification and labeling of Gal4-VP16 activators

To prepare fluorescently labeled Gal4-VP16^{649}, we first prepared a Gal4-SNAP-VP16 construct as described in ref. 51: A bacterial expression construct that encodes a fusion protein consisting of the yeast Gal4 DNA binding domain (amino acids 1-95), SNAPf[90], and the VP16 transcriptional activation domain[52], was subcloned in the pRJR plasmid[91] and was transformed into the BL21 (codon+, DE3) E. coli strain. Cells were grown in LB at 37°C until the OD_{600} reached 0.5. Protein was then induced with 0.1 mM IPTG and 10 μM $ZnCl_2$ at 30 °C for 3 hours. Cells were harvested by centrifugation at 5,000 rpm (096-041053, Thermo Scientific) for 10 minutes at 4°C, resuspended in Lysis buffer (20 mM HEPES-KOH pH 7.6, 10 μM $ZnCl_2$, 300 mM KCl, 5% (v/v) glycerol, 0.1% NP-40, and 1 mM PMSF), and lysed by sonication. The lysate was centrifuged at 15,000 rpm (096-124022, Thermo) for 15 minutes at 4°C and the supernatant was incubated with Ni-NTA agarose (Gold Biotechnology) at 4°C overnight on a rotator. The activator-bound beads were extensively washed with Wash buffer (20 mM HEPES-KOH pH 7.6, 10 μM $ZnCl_2$, 30 mM KCl, 5% (v/v) glycerol, 15 mM imidazole, and 1 mM PMSF), and protein eluted with Elution buffer (20 mM HEPES-KOH pH 7.6, 10 μM $ZnCl_2$, 30 mM KCl, 5% (v/v) glycerol, 600 mM imidazole, and 1 mM PMSF). Protein was further purified by salt gradient ion exchange chromatography using a Mono Q 5/50 GL column (GE healthcare) and Gradient buffers (20 mM HEPES-KOH pH 7.6, 0.1 M (low salt) or 1 M (high salt) NaCl, 10 μM $ZnCl_2$, 1 mM EDTA, 20% (v/v) glycerol, 1 mM DTT, and 1 μg/ mL each of aprotinin, leupeptin, pepstatin A, and benzamidine), and dialyzed against Dialysis buffer (20 mM HEPES-KOH pH 7.6, 500 mM KOAc, 10 uM $ZnCl_2$, 1 mM EDTA, and 20% (v/v) glycerol).

Purified Gal4-SNAP-VP16 was labeled with SNAP-Surface-649 dye (New England Biolabs) as in ([51]). Roughly 5 μM protein was incubated with 13.5 μM dye in PBS supplemented with 1 mM DTT at 4°C for 90 minutes. Labeled protein was incubated with Ni-NTA agarose at 4°C for 1 hour. The protein-coupled beads were extensively washed with PBS (supplemented with 10 % glycerol, 1 mM DTT, 10 μM $ZnCl_2$, and 1 μg/ mL each of aprotinin, leupeptin, pepstatin A, and antipain) to remove unincorporated dye. Then, labeled Gal4-VP16^{649} was eluted with PBS (supplemented with 10 % glycerol, 300 mM imidazole, 1 mM DTT, 10 μM $ZnCl_2$, and 1 μg/ mL each of aprotinin, leupeptin, pepstatin A, and antipain).

Unlabeled Gal4-VP16 was prepared as in refs. [49,50].

Yeast growth rate assays

Yeast cultures were diluted in YPD to OD_{600} of 0.002. Multiple replicate 150 - 200 μL wells of each strain were grown with orbital agitation at 30°C for 300,000 s in a Tecan microtiter plate reader. Log phase growth rates were measured as the slope of the linear portion of the $\log_2(OD_{600})$ records, then normalized to the growth rate of corresponding wild-type strain (**Figure S1B**). Records without a clearly defined log phase were discarded.

Preparation of yeast nuclear extracts

Yeast nuclear extracts were prepared as previously described[49], with minor modifications. Yeast strains (**Table S1**) were grown in 4 L of modified YPD (1% yeast extract, 2% peptone, 3% dextrose, 0.015% tryptophan, and 0.006% adenine) at 30°C until the absorbance at 600 nm reached 3. Cells were harvested by centrifugation at 4,000 rpm for 8 minutes at 4°C and resuspended in 150 mL TD buffer (50 mM Tris-HCl pH7.5 and 30 mM DTT). After 15 minutes incubation with gentle shaking at 30°C, cells were pelleted by centrifugation at 4,000 rpm for 12 minutes at 25°C and resuspended in 20 mL YPD/S (1% yeast extract, 2% peptone, 2% dextrose, and 1 M sorbitol). We then added 15 mg of Zymolyase 100T (120493-1, Amsbio) dissolved in 30 mL of 1 M sorbitol to make spheroplasts and incubated for 30-60 min with gentle shaking at 30°C. Spheroplasts were mixed with an additional 100 mL of YPD/S and pelleted by centrifugation at 4,000 rpm for 12 minutes at 25°C. This pellet was resuspended in 250 mL YPD/S and incubated at 30°C for 30 minutes for recovery. Then spheroplasts were washed first with YPD/S and then with cold 1 M Sorbitol by sequential centrifugations at 4,000 rpm for 12 minutes at 4°C and then resuspended in Buffer A (18% (w/v) Ficoll 400, 10 mM Tris-HCl pH 7.5, 20 mM KOAc, 5 mM $Mg(OAc)_2$, 1 mM EDTA pH 8.0, 0.5 mM spermidine, 0.17 mM spermine, 3 mM DTT, and 1 μg / mL each of aprotinin, leupeptin, pepstatin A, and antipain) and homogenized (62400-802, Wheaton). By four sequential centrifugations at a low speed (twice at 5,000 rpm for 8 minutes, then twice at 5,000 rpm for 5 minutes, with new centrifuge tubes used for each spin), large cell debris and improperly lysed spheroplasts were removed as pellets. The final supernatant was centrifuged at 13,000 rpm for 30 minutes at 4°C to collect crude nuclei. The nuclei were resuspended in 10 mL of Buffer B (100 mM Tris-OAc pH 7.9, 50 mM KOAc, 10 mM $MgSO_4$, 10% Glycerol, 2 mM EDTA pH 8.0, 3 mM DTT, and 1 μg/ mL each of aprotinin, leupeptin, pepstatin A, and antipain) and lysed by addition of 3 M $(NH_4)_2SO_4$ to a final concentration of 0.5 M. After 30 minutes incubation at 4°C on a rotator, the lysed nuclei were centrifuged at 37,000 rpm (type 70 Ti, Beckman) for 90 minutes at 4°C. The nuclear proteins in the supernatant were then precipitated by a gentle addition of granular $(NH_4)_2SO_4$ to ~ 75 % saturation (0.35 g per 1 mL of supernatant) with 30 minutes incubation on a rotator at 4 °C. Nuclear proteins were collected by centrifugation at 13,000 rpm for 20 minutes discarding the supernatant, and centrifuging the pellet again for 5 minutes and again discarding supernatant. The pellet (~0.8 g) was suspended in 2 mL of Buffer C (20 mM HEPES-KOH pH 7.6, 10 mM $MgSO_4$, 1 mM EGTA pH 8.0, 10% glycerol, 3 mM DTT, and 1 μg/ mL each of aprotinin, leupeptin, pepstatin A, and antipain). SNAP-fused proteins in the extract were then labeled by incubation with 0.4 μM SNAP-Surface-549 (New England Biolabs) for 1 hour at 4°C on a rotator. The labeled nuclear extract was dialyzed against Buffer C supplemented with 75 mM $(NH_4)_2SO_4$ or 100 mM KOAc in dialysis tubing (molecular weight cut-off, 6-8 kDa) three times (60 minutes, 90 minutes, and 120 minutes sequentially). Unincorporated free dye in the nuclear extract was mostly removed by incubation with recombinant SNAPf-coupled agarose beads (Pierce 26196) at 4°C for 1 hour. The agarose beads in the nuclear extract were then removed by centrifugation at 1,000 x *g* for 2 minutes at 4 °C. The labeled nuclear extract was flash frozen, aliquoted, and stored at -80°C.

Western blots

5 μL yeast nuclear extract was diluted 10-fold in 0.1% SDS, resolved by gel electrophoresis on a 10% SDS-PAGE gel, and transferred to a PVDF membrane (IPFL00010, Millipore). Anti-HA antibody (Roche, 12013819001) and anti-Rpb1 antibody (8WG16) were used for chemiluminescent detection of Med7 and Rpb1, respectively (**Figure S1C**).

In vitro transcription activity assay

The *in vitro* bulk transcription activity assay was performed as previously described[48,49]. In brief, 250 ng SB649 plasmid[92], 200 ng Gal4-VP16, and 10-50 μg yeast nuclear extract were incubated in ATB buffer (20 mM HEPES-KOH pH 7.6, 100 mM KOAc, 1 mM EDTA pH 8.0, and 5 mM $Mg(OAc)_2$) supplemented with 10 mM phosphocreatine, 0.1-0.2 units of creatine kinase, and 0.33 units of RNAsin (Promega) at room temperature for 5

minutes. Then, 500 μM ATP, 500 μM CTP, 20 μM UTP, and 0.3 μCi of α-^{32}P UTP (PerkinElmer) were added to the reaction to initiate transcription and label transcripts. After 45 minutes incubation at room temperature, transcripts were recovered by phenol/chloroform extraction, resolved by gel electrophoresis (8 M urea-6% polyacrylamide gel), and phosphoimaged on a Typhoon imager (GE Healthcare).

Preparation of DNA templates for microscope experiments

The UAS+promoter DNA template was prepared by PCR using Herculase II Fusion DNA Polymerase (Agilent #600675) from the SB649 plasmid[92] and upstream primer 5′-biotin-TTGGGTAACGCCAGGGT-3′ (IDT) and downstream primer 5′-Alexa488-AGCGGATAACAATTTCACACAG-3′. The UAS-only DNA template[49] was prepared the same way except with the downstream primer 5′-Alexa488-CGAGATCCTCTAGAGTCGG-3′. The promoter-only DNA template was amplified from the SB1958 plasmid using the same primers as the UAS+promoter DNA. The PCR product was purified using DNA SizeSelector-I SPRI magnetic beads (Aline Biosciences Z-6001) according to the manufacturer's instructions. Plasmid SB1958 is identical to plasmid SB649 except that the Gal4 binding sites have been mutated. Sequences for each template are given in **Table S2**.

Colocalization single-molecule microscopy

As previously described[49,50], we passivated glass coverslips using mPEG-SG-2000:biotin-PEG-SVA5000 (Laysan Bio) at a 200:1 ratio, then created flow chambers by sandwiching lines of silicone vacuum grease between two coverslips. We filled the chambers with KOBS buffer (50 mM Tris-OAc (pH 8.0), 100 mM KOAc, 8 mM $Mg(OAc)_2$, 27 mM $(NH_4)_2SO_4$, 0.1 mg/ mL bovine serum albumin (#126615 EMD Chemicals; La Jolla, CA)), and mounted them on a micro-mirror multi-wavelength TIRF microscope[46], using excitation wavelengths of 488 nm, 532 nm, and 633 nm. We first photobleached any fluorescent impurities on the coverslip surface by simultaneously irradiating with 2 mW at each of the three wavelengths (all laser powers were measured at the input to the micro-mirrors). We then added streptavidin-coated fluorescent beads (TransFluoSpheres, Thermofisher Scientific T10711) to serve as fiducial markers for drift correction[46]. The slide surface was then treated with 0.13 mg/mL NeutrAvidin (Thermofisher Scientific 31000) for one minute before being flushed with 20 μL KOBS buffer. We then introduced KOBS supplemented with ~10 pM biotinylated and AF488-labeled DNA template, an oxygen-scavenging system (0.9 units/mL protocatechuate dioxygenase [Sigma-Aldrich P8279], 5 mM protocatechuic acid [Sigma-Aldrich 03930590]), triplet state quenchers[93] (0.5 mM propyl gallate, 1 mM Trolox, 1 mM 4-nitrobenzyl alcohol)[94] and 0.5% dimethylsulfoxide. Images of the DNA were acquired using the 488 nm laser at 1.2 – 1.3 mW. In experiments with multiple DNA templates (*e.g.*, UAS+promoter and UAS-only DNA), the DNAs were sequentially added and images were taken with only the first DNA template in the sample and then with both templates in the sample[95]. Finally, the reaction mix containing yeast nuclear extract, reagents, and buffers with the following final concentrations was introduced: 5.5 mg protein/mL yeast nuclear extract, the same oxygen scavenging system and triplet state quenchers as previously detailed, 20 nM Cy5-TMP (if labeling Rpb1-DHFR), 0 – 50 nM labeled Gal4-VP16^{649} or 190 nM unlabeled Gal4-VP16, NTP depletion system (20 mM glucose and 2 units hexokinase [Sigma H4502]), 20 μM Acetyl-CoA, and 20 ng/μL competitor *E. coli* genomic DNA fragments[49], and buffer components (100.5 mM potassium acetate, 24.1 mM HEPES, pH 7.6, 0.4 mM Tris-acetate, 1 mM EDTA, 5 mM magnesium acetate, 2mM $MgSO_4$, 0.2 mM EGTA, 15 mM $(NH_4)_2SO_4$, 4.25% glycerol).

For experiments with Gal4-VP16^{649} and Med7^{549}, separate images using 633 nm and 532 nm excitation (0.5 and 1.2 mW, respectively) were captured every 1.4 s (0.5 s for each channel, plus switching times) (**Figures 2** and **5**). For experiments with Rpb1^{Cy5} and Med7^{549}, separate 633 nm and 532 nm excitation (0.4 and 0.8 mW, respectively) images were captured every 2.7 s (1 s per frame for each channel, plus switching times) (**Figures 3** and **4**; **Table S2**). Custom software Glimpse (github.com/gelles-brandeis/Glimpse) was used to operate the microscope, laser shutters, filter wheels, and camera.

Surface-tethered DNA detachment/cleavage rate

To measure the rate at which surface-tethered DNA molecules detached from or were cleaved off of the chamber surface (**Figure S4D**) under the conditions of the CoSMoS experiments, we first prepared chambers with surface-tethered DNA in KOBS buffer with oxygen-scavenging and triplet state quencher as described for CoSMoS experiments for DNA imaging. After imaging the DNA, we added YNE in the same reaction mix as described previously minus activator and Cy5-TMP). This step was omitted for the zero-exposure control. After zero, 900, or 2,280 s exposure to yeast nuclear extract, the chamber was washed with the full CoSMoS reaction mixture (including 190 nM activator) and the DNA was immediately reimaged. The fraction of DNA molecules in the first image that had survived in the second image was normalized by the surviving fraction in the zero-exposure experiment.

CoSMoS image analysis

Microscope images were preprocessed as previously described[47]. In brief, DNA spots were first detected in the blue-excited channel and their centers determined via Gaussian fitting. These locations were then mapped to the red- and green-excited "binder"[47] protein channels and corrected for spatial drift across the time duration of the experiment using the fluorescent beads as fiducial markers. When two DNA templates were present in the same sample (e.g., both UAS+promoter and UAS-only DNAs), multiple blue channel images pre- and post-addition of the second DNA were used to distinguish between the two[95]. Locations lacking visible DNA molecules were also randomly selected as described[47], to serve as controls to measure DNA-independent non-specific interactions of binder proteins with the slide surface. The fluorescence intensity values from the binder protein channels at DNA and no-DNA locations were integrated to create time records (e.g., **Figure 2A-C**; **Figure 4A**). Presence or absence of each binder protein at each DNA location in each frame was determined by analysis of the two-dimensional image data using the spot-detection method described previously[47]. The resulting binary bound/unbound state records were used to generate rastergrams (**Figures 2E-F; 3A-E; 4B; S2; S4A-B; S5A-B**).

Mediator association rate constant

To measure DNA-specific rate constants for Mediator association (**Figure 3F-H**, **Table S2**), we measured the time from the beginning of the experiment until the first time a Med7^{649} molecule was detected at each DNA or no-DNA location. Restricting analysis to the first binding at each location reduces confounding effects (e.g., from photobleaching, dye blinking, or incomplete labeling) on the measurement[47]. In the distributions of times to first binding, a minority subpopulation of DNA locations appeared to become incapable of DNA-specific Med7^{649} association, and the size of this subpopulation was lower in experiments that displayed higher DNA-specific binding rates.

This observation suggests kinetic competition between DNA-specific Med7^{649} association and inhibitory processes that cause DNA locations to become refractory to association. Control experiments show that a fraction of these apparently inactive locations could be caused by DNA detachment from the surface or DNA endonucleolytic cleavage before Mediator has had a chance to bind (**Figure S4D**). However, detachment or cleavage is insufficient to account for most inactive locations. We propose instead that most of the inactive DNAs instead result from occlusion of the DNA molecules by interactions with DNA-binding proteins (e.g., histones[48]) present in the

YNE, or by non-specific interactions of the DNA molecules with the slide surface, either of which could obstruct Mediator binding. To account for these inhibitory "DNA inactivation" processes, we analyzed the time-to-first-binding data using the model

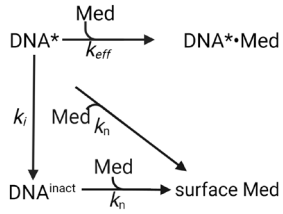

which assumes that DNA locations recorded before extract addition are initially in a state (DNA*) that is binding-competent, are slowly converted (at rate k_i) to inactive locations DNA^{inact}. Only DNA* locations are capable of specific association with Mediator (Med). Specific binding (with apparent first-order rate constant k_{eff}) forms the specific complex DNA*•Med. In contrast, both DNA* and DNA^{inact} locations will exhibit non-specific surface binding (forming "surface Med") with apparent first-order rate constant k_n. This model predicts the conditional probability of observing a time interval t until first Med7^{649} binding, given specified values for the rate constants, is proportional to:

$$p(t \mid k_{\text{eff}}, k_{\text{i}}, k_{\text{n}}) = \left[\frac{k_{\text{eff}}}{(k_{\text{eff}}+k_{\text{i}})} - \frac{n_z}{N}\right](k_{\text{eff}} + k_{\text{n}} + k_{\text{i}})e^{-(k_{\text{eff}}+k_{\text{n}}+k_{\text{i}})t} + \left[\frac{k_{\text{i}}}{(k_{\text{eff}}+k_{\text{i}})}\right](k_{\text{n}})e^{-(k_{\text{n}})t},$$

(Equation 1)

where $^{n_z}/_{N}$ is the fraction of DNA locations at which a binder molecule was already present at the start of acquisition. To determine the rate constants k_{eff}, k_i, and k_n, we adapted the method in Eqs. 4–7 of ref. 47, which are reparameterized as $A_f(t) \equiv \frac{k_{\text{eff}}}{(k_{\text{eff}}+k_{\text{i}})}$ and $k_{on} \equiv k_{\text{eff}} + k_{\text{i}}$. We first used maximum likelihood fitting to determine k_n from data taken at control no-DNA locations. Holding k_n at this value, we then determined A_f and k_{on} from data at DNA locations. Finally, k_{eff} and k_i were calculated as $k_{eff} = k_{on} \times A_f$ and $k_i = k_{on}$ (1 - A_f). Parameter values with S.E. calculated by bootstrapping (1,000 samples) are reported in **Table S2.** Values of k_i could only be accurately determined in experimental conditions (UAS-containing DNA and Gal4-VP16 present) that showed specific Med7^{649} binding to DNA. In those experiments the value of k_i was consistently around $1–2 \times 10^{-3}$ s^{-1} (**Table S2**), consistent with the model assumption of a constant rate of time-dependent DNA inactivation.

Mediator dwell times

Frequency distributions of Med7^{649} specific-binding dwell times on DNA (**Figure 2J**) were determined by subtracting the distribution measured at randomly selected no-DNA locations from the distribution at DNA locations measured from the same recording[47]. Only dwells for which the end of the dwell was observed during the experiment were used in this analysis. Distributions were plotted as cumulative dwell time frequency distributions or as binned dwell time probability density distributions.

Measured dwell times were fit to a multi-exponential model, using an analogous approach to that described by Equations 9 – 12 in ref. 47 (**Figure S4E-F**). First, dwells from non-specific Mediator binding to the slide surface at no-DNA locations were fit using the biexponential empirical probability density model

$$P_B(t \mid a_B, \tau_{B1}, \tau_{B2}) = \left(\frac{1}{a_B A_B + (1-a_B)B_B}\right)\left(a_B \frac{e^{-\frac{t}{\tau_{B1}}}}{\tau_{B1}} + (1 - a_B)\frac{e^{-\frac{t}{\tau_{B2}}}}{\tau_{B2}}\right),$$

(Equation 2)

with $A_B = e^{\left(-t_{min}/\tau_{B1}\right)} - e^{\left(-t_{max}/\tau_{B1}\right)}$ and $B_B = e^{\left(-t_{min}/\tau_{B2}\right)} - e^{\left(-t_{max}/\tau_{B2}\right)}$. The variables t_{min} and t_{max} were set to the minimum and maximum interval lengths that can be resolved in the experiment. The two exponential components have characteristic lifetimes τ_{B1} and τ_{B2} and amplitudes a_B and (1-a_B). The corresponding likelihood function was maximized to obtain values for a_B, τ_{B1}, and τ_{B2}.

Next, dwells from DNA locations were fit to triexponential empirical probability density model for DNA-specific Mediator binding that also includes the biexponential non-specific surface binding determined from no-DNA locations

$$P(t \mid a_S, a_M, \tau_S, \tau_M, \tau_L) = \frac{1}{f_{data+bk}}\left[\begin{array}{c}(f_{data+bk} - f_{bk})\left(\frac{1}{a_S A + a_M B + (1-a_S-a_M)C}\right)\left(\frac{a_S e^{-t/\tau_S}}{\tau_S} + \frac{a_M e^{-t/\tau_M}}{\tau_M} + \frac{(1-a_S-a_M)e^{-t/\tau_L}}{\tau_L}\right) \\ + f_{bk}\left(\frac{1}{a_B A_B + (1-a_B)B_B}\right)\left(a_B \frac{e^{-\frac{t}{\tau_{B1}}}}{\tau_{B1}} + (1 - a_B)\frac{e^{-\frac{t}{\tau_{B2}}}}{\tau_{B2}}\right)\end{array}\right],$$

(Equation 3)

with $A = e^{\left(-t_{min}/\tau_S\right)} - e^{\left(-t_{max}/\tau_S\right)}$; $B = e^{\left(-t_{min}/\tau_M\right)} - e^{\left(-t_{max}/\tau_M\right)}$; and $C = e^{\left(-t_{min}/\tau_L\right)} - e^{\left(-t_{max}/\tau_L\right)}$. The variables $f_{data+bk}$ and f_{bk} were set to the frequencies of Mediator binding events measured at DNA and no-DNA locations, respectively. The three exponential components have characteristic lifetimes τ_S, τ_M, and τ_L and amplitudes a_S, a_M, and $a_L = (1 - a_S - a_M)$. This corresponding likelihood equation maximized to determine values for the parameters τ_S, τ_M, and τ_L, a_S, and a_M.

Binding rate enhancement

To measure the acceleration by the presence of Mediator on the DNA binding of RNApII, we counted the number of time points in a single-molecule experiment in which RNApII arrived at a DNA location at which Mediator was already bound, $N_{\text{Med->Med-RNApII}} \equiv N_{\text{recruited}}$, and the analogous number of RNApII arrivals when Mediator was not already bound, $N_{\text{Ø->RNApII}} \equiv N_{\text{non-recruited}}$. We then calculated the recruited and non-recruited RNApII binding frequencies as $f_r = N_{\text{recruited}} / t_{\text{Med}}$ and $f_{nr} = N_{\text{non-recruited}} / t_{Ø}$, respectively, where t_{Med} is the number of time points at which Mediator, but not RNApII, was present and $t_{Ø}$ is the number of time points at which neither Mediator nor RNApII was present. The subset of binding events in which Med7^{549} and Rpb1^{Cy5} arrived within 2.7 s of each other were excluded from this analysis. We also calculated an analogous quantity f_{non} for control no-DNA locations to account for the non-specific binding of Mediator. The DNA-specific binding rate enhancement (**Figure 4C**, solid green bars) was taken to be

$$P = \frac{(f_r - f_{\text{non}})}{(f_{\text{nr}} - f_{\text{non}})},$$

(Equation 4)

where $P = 1$ indicates equal preference for the two binding modes. To check that P > 1 values were not coincidental, we also performed randomized control analyses in which Mediator and RNApII records from different DNA locations were randomly selected without replacement and paired for the P calculation. These controls yielded $P \approx 1$ (**Figure 4C**, striped green bars) confirming the detected preferences were not biased by kinetic differences between the proteins studied. These steps were repeated to analyze the recruitment of Mediator by RNApII, with opposite designations (**Figure 4C**, solid and striped red bars). In **Figure 4C** left, the binding rate enhancement values are calculated from DNA-specific RNApII binding frequencies of Med7^{549} and Rpb1^{Cy5} to UAS+promoter DNA in the experiment in **Figure 4A** plus two additional replicates. In **Figure 4C** right they are calculated from a single replicate experiment with UAS-only DNA. $N_{\text{recruited}}$ and $N_{\text{non-recruited}}$ are the total number of observed Rpb1^{Cy5} binding events observed to DNA molecules with and without bound Med7^{549}, respectively (**Figure 4C**, green bars), or the reverse (**Figure 4C**, red bars).

Simultaneous arrival of Mediator and RNApII at DNA molecules

Mediator and RNApII were scored as arriving simultaneously (**Figure 4D**; **Figure S5C-D**) if appearance of Med7^{549} and Rpb1^{Cy5} fluorescence at a DNA location occurred within the experimental time resolution (± 2.7 s). Control analyses of the same 100 randomly selected first-binding datasets in **Figure 4D** in which a random time offset (uniformly distributed between −133 and +133 seconds) was introduced between the Rpb1^{Cy5} and Med7^{549} record

from each DNA location exhibited zero simultaneous arrivals, indicating that the observed simultaneous arrivals of Med7^{549} and Rpb1^{Cy5} were not coincidental.

To test the idea that apparently simultaneous arrivals of Med7^{549} and Rpb1^{Cy5} reflected recruitment of a pre-formed complex containing both proteins, rather than independent sequential binding of the two proteins within the time resolution of the experiment, we quantitatively examined the formation of Mediator and RNApII ternary complexes. Ternary complexes were defined using time intervals in which both Med7^{549} and Rpb1^{Cy5} were simultaneously present for at least one shared frame. To minimize the effect of Cy5-TMP blinking, only a single Rpb1^{Cy5} event was considered per Med7^{549} dwell (for example, see **Figure 4A**, top trace between 0 – 600 seconds). Ternary complex formation events were then categorized as in **Figure S5C-D** (bars). The kinetically modeled sequential events (red and green fit curves) were substantially lower than the blue bars when extrapolated to zero time-difference, indicating that the vast majority of these apparently simultaneous arrivals were indeed simultaneous. The analogous analysis was performed for simultaneous departures (**Figure S5E-F**).

Gal4-VP16^{649} and Med7^{549} spot presence and spot fluorescence intensity

CoSMoS experiments with Med7^{549} and 0, 10, 25, or 50 nM Gal4-VP16^{649} or 190 nM unlabeled Gal4-VP16 were processed by the Bayesian machine learning method implemented in the software *tapqir* using the described time-independent *cosmos* model[63]. To measure the fraction of DNA molecules colocalized with a Gal4-VP16^{649} or Med7^{549} fluorescence spot in these experiments (**Figure S6C**), we scored time points at each DNA location with a DNA-specific Gal4-VP16^{649} and/or Med7^{549} spot as those with specific spot probability $p_{\text{specific}} \geq 0.5$. In the experiment with no Gal4-VP16^{649}, the fraction of DNAs with a colocalized Gal4-VP16^{649} spot was taken to be zero (leading to the solid red points in **Figure 5A; Figure 6B, D, F;** and **Figure S6C**).

The *cosmos* model fits two candidate spots per frame per DNA location. For both candidates it calculates the probabilities $p(\theta = 1)$ and $p(\theta = 2)$ (denoted *theta_probs* in ref. 96) that candidate spots 1 and 2 are authentic, target-specific spots[63]. To accommodate cases in which a single, DNA-colocalized spot was fit as consisting of two overlapping candidate spots, we take the intensity (in photons) above background of all target-specific (i.e., $p_{\text{specific}} \geq 0.5$) spots to be

$$I = \frac{p(\theta = 1) \cdot h_1 + p(\theta = 2) \cdot h_2}{g \cdot [p(\theta = 1) + p(\theta = 2)]},$$

(Equation 5)

where the *cosmos* model parameters h_1 and h_2 are the integrated Gaussian-modeled spot intensities for spots 1 and 2; and g is camera gain (ADU/photon). This theta probability weighting means the intensity value will reflect the "true" spot when the choice is clear or combine the signals when a single intense spot is modeled as two overlapping spots. To calculate the time-dependence of the average Gal4-VP16^{649} and Med7^{549} fluorescence per DNA molecule (**Figure S6A, B**, respectively), we binned the experimental timepoints into quintiles (10, 25, 50 nM Gal4-VP16) or deciles (190 nM Gal4-VP16; see **Table S3**). For all DNA locations at all timepoints in each bin, we averaged the spot intensity I (Equation 5) if a target-specific spot was detected (i.e., $p_{\text{specific}} \geq 0.5$) or a value of zero if no spot was detected ($p_{\text{specific}} < 0.5$). Standard errors of this mean were conservatively estimated using the number of DNA molecules, N_{DNA} (i.e., they did not account for the number of time points), since successive measurements on the same DNA location are not fully statistically independent.

Fitting spot intensity distributions

The molecular complexes studied may in general contain more than one Gal4-VP16 or Mediator and therefore may contain more than one dye-labeled Gal4-VP16^{649} or Med7^{549} protein. To measure the fluorescence intensities, distributions of target-specific fluorescence spot intensity I across multiple time points and DNA locations (e.g., **Figure S3)** were maximum likelihood fit to the gamma distribution mixture model probability density function

$$\sum_{i=1}^{j}\left[P_i \frac{1}{w^{-\mu_i w}\Gamma(\mu_i w)} I^{\mu_i w - 1} e^{-wI}\right],$$

(Equation 6)

where j was set at a fixed number of components corresponding to the maximum number of dyes per spot; μ_i was taken to be $i \cdot \mu_1$ for $i = 2,\ldots j$; and the fit parameters were μ_1, the mean intensity above background of a single dye moiety; w, the gamma distribution inverse scale parameter; and P_i for $i = 1,\ldots j$, the fractional amplitude of the i^{th} component, where $\sum_{i=1}^{j}[P_i] = 1$. All fits, fit parameter values, and parameter standard errors are reported in **Supplementary Data File 1.**

Gal4-VP16^{649} and Med7^{549} fraction labeled

The fraction of Gal4-VP16 dimers in the Gal4-VP16^{649} preparation that contained one or more fluorescent dye was measured from the distribution of fluorescence intensity changes accompanying the first Gal4-VP16^{649} binding seen at each DNA location in the 10 nM Gal4-VP16^{649} experiment (**Figure 2A**). In the first instance of three consecutive Gal4-VP16^{649}-present ($p_{\text{specific}} \geq 0.5$) frames immediately following a Gal4-VP16^{649}-absent ($p_{\text{specific}} < 0.5$) frame, we used the intensity above background I (Equation 5) values for the second $p_{\text{specific}} \geq 0.5$ frame. The distribution of these intensities was fit to Equation 6 as described above, using $j = 4$ (**Figure S3A)**. Gal4-VP16 binds tightly to its cognate DNA sequence as a dimer, so we assume that the first and second gamma components correspond to dimers with one or two fluorescent dyes, respectively, while the much smaller amplitude third and fourth gamma components are due to outlier events, e.g., instances in which two dimers bound in rapid succession. The subunit labeling fraction was calculated as

$$f_{\text{Gal4-VP16 monomers}} = \frac{2P_2}{P_1 + 2P_2},$$

(Equation 7)

and the fraction of dimers with at least one dye was then calculated as

$$f_{\text{Gal4-VP16 dimers}} = 1 - (1 - f_{\text{Gal4-VP16 monomers}})^2.$$

(Equation 8)

The reported experiments used a single Gal4-VP16^{649} preparation with $f_{\text{Gal4-VP16 monomers}} = 82 \pm 11\%$ and $f_{\text{Gal4-VP16 dimers}} = 97 \pm 4\%$.

We estimated a lower limit on the fraction of dye-labeled Mediator molecules in the Med7^{549}/Rpb1^{Cy5} extract from the ratio of background-corrected frequencies for Rpb1^{Cy5} arrival when Med7^{549} was present to when it was absent intervals, which is the 14.6 ± 1.0 recruitment preference (**Figure 4C**, left, green bar). This corresponds to a lower limit Med^{549} labeling fraction of $\bar{f}_{\text{Mediator}} = 14.6 / (14.6 + 1) = 94\%$.

Number of Gal4-VP16 or Med7 molecules per DNA

To calculate the average number of Gal4-VP16 or Med7 on each DNA at equilibrium (**Figure 5A**, points; **Figure 6**, points), I (Equation 5) distributions were fit to Equation 6, using values of j chosen to account for the observed distributions while using the smallest number of components to prevent overparameterization: Gal4-VP16^{649} intensities were fit using $j = 8$ or 10; and Med7^{549} intensities were fit with $j = 4$ (**Supplementary Data File 1**). For Gal4-VP16^{649}, equilibrium μ_1 values were similar at all concentrations and were similar to μ_1 measured earlier from the first binding event data (compare **Figure S3A** with **Figure S3B** and **Supplementary Data File 1)**, consistent with the fitting procedure accurately measuring the single-dye intensity values in the equilibrium intensity distributions. The μ_1 values for the equilibrium Med7^{549} intensity distributions from the experiments with 10, 25, and 50 nM Gal4-VP16^{649} were also consistent with each other, but not with data at 190 nM activator, which was collected under different acquisition conditions as described earlier. At 0 nM Gal4-VP16^{649},

there was not enough Med7^{549} binding to fit an intensity distribution to the Gamma mixture model, so all instances of binding were assumed to have one Med7^{549} molecule present. We calculated the average number of dye molecules per fluorescent spot as

$$d = \sum_{i=1}^{j} [i\ P_i].$$

(Equation 9)

The fraction of uncleaved DNA molecules remaining on the slide surface during the equilibrium time intervals, each of which was centered at t_c = ~1,250 s from the start of the experiment, was estimated as $f_{DNA} = e^{-(k_L\ t_c)} = 0.75$, where $k_L = 2.3 \times 10^{-4}$ s^{-1} is the independently determined rate of DNA loss from the surface (**Figure S4D**). The mean numbers of Gal4-VP16 dimers and Mediator complexes per surviving DNA location were then calculated as

$$(d \bullet f_{\geq 1\ \text{Gal4-VP16}}) / (2\ f_{\text{Gal4-VP16 monomers}})(f_{\text{DNA}}),$$

(Equation 10)

and

$$(d \bullet f_{\geq 1\ \text{Mediator}}) / (\bar{f}_{\text{Mediator}})(f_{\text{DNA}}),$$

(Equation 11)

respectively, where $f_{\geq 1\ \text{Gal-VP16}}$ and $f_{\geq 1\ \text{Mediator}}$ are the fractions of original DNA locations with one or more dye-labeled Gal4-VP16^{649} and Mediator^{549} (**Figure 5A**).

Quantitative models for Mediator recruitment by Gal4-VP16

To test quantitative explanations for the observed activator binding and Mediator recruitment by activator to a DNA containing five identical Gal4 binding sites, we formulated three contrasting equilibrium statistical mechanics models: two "single-bridging" models with either noninteracting or interacting TA molecules (**Figures 6A** and **C**, respectively) and a "multiple-bridging" model (**Figure 6E)**. For each model, we enumerated all possible protein-bound states of a DNA molecule and calculated the associated statistical weights from the free energy contributions of the protein-DNA and protein-protein interactions present and the state multiplicity[17]. The probability of a DNA being in a given state at equilibrium is its statistical weight divided by the sum of all weights. In each model, the state probabilities depend on the free concentration of Gal4-VP16, [A] (which is assumed to be equal to the total added Gal4-VP16 or Gal4-VP16^{649}), and either two or three variable parameters.

In the independent single-bridging model (**Figure 6A**), in which only one TA at a time can interact with Mediator, only two parameters were needed: K_a, the equilibrium constant for association of a TA dimer with a single Gal4 binding site on the DNA; and $m = [M]K_m$, where [M] is the concentration of Mediator and K_m is the equilibrium constant for association of a single Mediator to a single TA dimer on DNA.

In the single-bridging model with TA interactions (**Figure 6C**), an additional parameter was introduced to reflect the interactions between TAs: $b = e^{-\left(\frac{G_a}{k_B T}\right)}$, the Boltzmann factor representing the strength of each TA interaction, where G_a is the free energy associated with interactions between a pair of neighboring TAs bound to a DNA.

For the multiple-bridging model (**Figure 6E**), state probabilities depend on the model parameters K_a, m, and additional parameter c. The parameter $c = e^{-\left(\frac{G_m}{k_B T}\right)}$ is the Boltzmann factor corresponding to the free energy G_m associated with the interaction between each of the second through fifth TAs and Mediator.

To determine the set of parameter values, $\vec{\beta}$, that give the best agreement between a model and the occupancy data, we used the MATLAB *fminsearch* function to minimize:

$$-\ln p = \tfrac{1}{2} \sum_{i=1}^{7} \left(\left[(y_i \mid \vec{\beta}) - x_i \right]^2 / \Delta x_i^{\,2} \right),$$

(Equation 12)

where p is the relative likelihood, the seven x_i values are the experimentally measured mean numbers of equilibrium activator dimers or Mediator molecules per DNA (the points shown for non-zero activator concentrations in **Figure 5A** and **Figure 6B, D,** and **F**), Δx_i is the standard error associated with each x_i, and $(y_i \mid \vec{\beta})$ are the corresponding model predictions for occupancy values given the set of model parameters. Parameter confidence intervals were determined by bootstrapping (1,000 samples).

For the multiple-bridging model the value of K_a determined from the fit (0.017 nM^{-1}) is of similar magnitude to a published measurement (0.067 nM^{-1}; ref. 97) for Gal4-DBD binding to its consensus DNA site at a somewhat different ionic strength. The fitting procedure estimates m, the product of Mediator concentration and its association constant with a single DNA-bound activator. Since single molecules cannot be detected by TIRF above solution concentrations of roughly 50 nM, the concentration of Mediator in our experiments is at or below that value. Thus, the fit value of m, 0.007, yields a predicted single activator-Mediator association equilibrium constant of $K_m \geq 0.14\ \mu M^{-1}$, in rough agreement with equilibrium constants reported for binding of Mediator to Gal4 and Gcn4 ADs[29,30,98].

Author contributions

J. Jeon made yeast nuclear extracts and labeled activator and performed microscopy experiments with labeled activator and Mediator. D. H. Zhou performed all other experiments. Statistical mechanical modeling and computation were performed by N. Farheen with contributions from D. H. Zhou, J. Kondev, and J. Gelles. D. H. Zhou performed microscopy image analysis with contributions from L. J. Friedman. The paper was written by D. H. Zhou and J. Gelles, with additional contributions and edits from the other authors. S. Buratowski and J. Gelles were responsible for project conception and funding acquisition.

Acknowledgements

We thank Grace Rosen and Inwha Baek for support in troubleshooting and method development; Doug Theobald & Yerdos Ordabayev for their help with maximum likelihood modeling, Yoo Jin Joo for the purified Gal4-VP16, and Johnson Chung for help with microscopy and data analysis. This work was supported by grants from the National Cancer Institute and the National Institute for General Medical Sciences: R01CA246500 to J.G. and S.B., R01GM081648 to J.G., and R01GM046498 to S.B.

Supplementary data files

Supplementary Data File 1: Fits of spot intensity distributions to 10- and 4-component Gamma mixture models (SupplementaryDataFile1.xlsx) (Related to Figure S3)

References

1. Reményi, A., Schöler, H.R., and Wilmanns, M. (2004). Combinatorial control of gene expression. Nat Struct Mol Biol *11*, 812–815. https://doi.org/10.1038/nsmb820.
2. Weake, V.M., and Workman, J.L. (2010). Inducible gene expression: diverse regulatory mechanisms. Nat Rev Genet *11*, 426–437. https://doi.org/10.1038/nrg2781.
3. Cramer, P. (2019). Organization and regulation of gene transcription. Nature *573*, 45–54. https://doi.org/10.1038/s41586-019-1517-4.
4. Struhl, K. (1991). Mechanisms for diversity in gene expression patterns. Neuron *7*, 177–181. https://doi.org/10.1016/0896-6273(91)90256-Y.
5. Sainsbury, S., Bernecky, C., and Cramer, P. (2015). Structural basis of transcription initiation by RNA polymerase II. Nat Rev Mol Cell Biol *16*, 129–143. https://doi.org/10.1038/nrm3952.

6. Lee, T.I., and Young, R.A. (2000). Transcription of Eukaryotic Protein-Coding Genes. Annu. Rev. Genet. *34*, 77–137. https://doi.org/10.1146/annurev.genet.34.1.77.
7. Ptashne, M., and Gann, A. (1997). Transcriptional activation by recruitment. Nature *386*, 569–577. https://doi.org/10.1038/386569a0.
8. Ptashne, M. (2005). Regulation of transcription: from lambda to eukaryotes. Trends Biochem Sci *30*, 275–279. https://doi.org/10.1016/j.tibs.2005.04.003.
9. Herschlag, D., and Johnson, F.B. (1993). Synergism in transcriptional activation: a kinetic view. Genes & Development *7*, 173–179. https://doi.org/10.1101/gad.7.2.173.
10. Lin, Y.-S., Carey, M., Ptashne, M., and Green, M.R. (1990). How different eukaryotic transcriptional activators can cooperate promiscuously. Nature *345*, 359–361. https://doi.org/10.1038/345359a0.
11. Carey, M. (1998). The Enhanceosome and Transcriptional Synergy. Cell *92*, 5–8. https://doi.org/10.1016/S0092-8674(00)80893-4.
12. Kim, S., and Wysocka, J. (2023). Deciphering the multi-scale, quantitative cis-regulatory code. Molecular Cell *83*, 373–392. https://doi.org/10.1016/j.molcel.2022.12.032.
13. Sharon, E., Kalma, Y., Sharp, A., Raveh-Sadka, T., Levo, M., Zeevi, D., Keren, L., Yakhini, Z., Weinberger, A., and Segal, E. (2012). Inferring gene regulatory logic from high-throughput measurements of thousands of systematically designed promoters. Nat Biotechnol *30*, 521–530. https://doi.org/10.1038/nbt.2205.
14. Spitz, F., and Furlong, E.E.M. (2012). Transcription factors: from enhancer binding to developmental control. Nat Rev Genet *13*, 613–626. https://doi.org/10.1038/nrg3207.
15. Giorgetti, L., Siggers, T., Tiana, G., Caprara, G., Notarbartolo, S., Corona, T., Pasparakis, M., Milani, P., Bulyk, M.L., and Natoli, G. (2010). Noncooperative Interactions between Transcription Factors and Clustered DNA Binding Sites Enable Graded Transcriptional Responses to Environmental Inputs. Molecular Cell *37*, 418–428. https://doi.org/10.1016/j.molcel.2010.01.016.
16. Scholes, C., DePace, A.H., and Sánchez, Á. (2017). Combinatorial Gene Regulation through Kinetic Control of the Transcription Cycle. Cell Systems *4*, 97-108.e9. https://doi.org/10.1016/j.cels.2016.11.012.
17. Bintu, L., Buchler, N.E., Garcia, H.G., Gerland, U., Hwa, T., Kondev, J., and Phillips, R. (2005). Transcriptional regulation by the numbers: models. Current Opinion in Genetics & Development *15*, 116–124. https://doi.org/10.1016/j.gde.2005.02.007.
18. Reiter, F., Wienerroither, S., and Stark, A. (2017). Combinatorial function of transcription factors and cofactors. Current Opinion in Genetics & Development *43*, 73–81. https://doi.org/10.1016/j.gde.2016.12.007.
19. Carey, M., Lin, Y.S., Green, M.R., and Ptashne, M. (1990). A mechanism for synergistic activation of a mammalian gene by GAL4 derivatives. Nature *345*, 361–364. https://doi.org/10.1038/345361a0.
20. Bhoite, L.T., Yu, Y., and Stillman, D.J. (2001). The Swi5 activator recruits the Mediator complex to the HO promoter without RNA polymerase II. Genes & Development *15*, 2457–2469. https://doi.org/10.1101/gad.921601.
21. Bryant, G.O., and Ptashne, M. (2003). Independent Recruitment In Vivo by Gal4 of Two Complexes Required for Transcription. Molecular Cell *11*, 1301–1309. https://doi.org/10.1016/S1097-2765(03)00144-8.
22. Holstege, F.C.P., Jennings, E.G., Wyrick, J.J., Lee, T.I., Hengartner, C.J., Green, M.R., Golub, T.R., Lander, E.S., and Young, R.A. (1998). Dissecting the Regulatory Circuitry of a Eukaryotic Genome. Cell *95*, 717–728. https://doi.org/10.1016/S0092-8674(00)81641-4.
23. Thompson, C.M., and Young, R.A. (1995). General requirement for RNA polymerase II holoenzymes in vivo. Proc Natl Acad Sci U S A *92*, 4587–4590.
24. Richter, W.F., Nayak, S., Iwasa, J., and Taatjes, D.J. (2022). The Mediator complex as a master regulator of transcription by RNA polymerase II. Nature Reviews Molecular Cell Biology *23*, 732–749. https://doi.org/10.1038/s41580-022-00498-3.
25. Chen, H., and Pugh, B.F. (2021). What do Transcription Factors Interact With? J Mol Biol *433*, 166883. https://doi.org/10.1016/j.jmb.2021.166883.
26. Poss, Z.C., Ebmeier, C.C., and Taatjes, D.J. (2013). The Mediator complex and transcription regulation. Critical Reviews in Biochemistry and Molecular Biology *48*, 575–608. https://doi.org/10.3109/10409238.2013.840259.
27. Allen, B.L., and Taatjes, D.J. (2015). The Mediator complex: a central integrator of transcription. Nat Rev Mol Cell Biol *16*, 155–166. https://doi.org/10.1038/nrm3951.
28. Warfield, L., Donczew, R., Mahendrawada, L., and Hahn, S. (2022). Yeast Mediator facilitates transcription initiation at most promoters via a Tail-independent mechanism. Mol Cell *82*, 4033-4048.e7. https://doi.org/10.1016/j.molcel.2022.09.016.
29. Herbig, E., Warfield, L., Fish, L., Fishburn, J., Knutson, B.A., Moorefield, B., Pacheco, D., and Hahn, S. (2010). Mechanism of Mediator Recruitment by Tandem Gcn4 Activation Domains and Three Gal11 Activator-Binding Domains. Mol Cell Biol *30*, 2376–2390. https://doi.org/10.1128/MCB.01046-09.
30. Tuttle, L.M., Pacheco, D., Warfield, L., Wilburn, D.B., Hahn, S., and Klevit, R.E. (2021). Mediator subunit Med15 dictates the conserved "fuzzy" binding mechanism of yeast transcription activators Gal4 and Gcn4. Nature Communications *12*, 2220. https://doi.org/10.1038/s41467-021-22441-4.
31. Sun, F., Sun, T., Kronenberg, M., Tan, X., Huang, C., and Carey, M.F. (2021). The Pol II preinitiation complex (PIC) influences Mediator binding but not promoter–enhancer looping. Genes & Development *35*, 1175–1189. https://doi.org/10.1101/gad.348471.121.
32. Knoll, E.R., Zhu, Z.I., Sarkar, D., Landsman, D., and Morse, R.H. (2018). Role of the pre-initiation complex in Mediator recruitment and dynamics. eLife *7*, e39633. https://doi.org/10.7554/eLife.39633.
33. Petrenko, N., Jin, Y., Wong, K.H., and Struhl, K. (2016). Mediator Undergoes a Compositional Change during Transcriptional Activation. Molecular Cell *64*, 443–454. https://doi.org/10.1016/j.molcel.2016.09.015.
34. Zhao, H., Li, J., Xiang, Y., Malik, S., Vartak, S.V., Veronezi, G.M.B., Young, N., Riney, M., Kalchschmidt, J., Conte, A., et al. (2024). An IDR-dependent mechanism for nuclear receptor control of Mediator interaction with RNA polymerase II. Molecular Cell *84*, 2648-2664.e10. https://doi.org/10.1016/j.molcel.2024.06.006.
35. Robinson, P.J., Trnka, M.J., Bushnell, D.A., Davis, R.E., Mattei, P.-J., Burlingame, A.L., and Kornberg, R.D. (2016). Structure of a Complete Mediator-RNA Polymerase II Pre-Initiation Complex. Cell *166*, 1411-1422.e16. https://doi.org/10.1016/j.cell.2016.08.050.
36. Plaschka, C., Larivière, L., Wenzeck, L., Seizl, M., Hemann, M., Tegunov, D., Petrotchenko, E.V., Borchers, C.H., Baumeister, W., Herzog, F., et al. (2015). Architecture of the RNA polymerase II–Mediator core initiation complex. Nature *518*, 376–380. https://doi.org/10.1038/nature14229.
37. Schilbach, S., Hantsche, M., Tegunov, D., Dienemann, C., Wigge, C., Urlaub, H., and Cramer, P. (2017). Structures of transcription pre-initiation complex with TFIIH and Mediator. Nature *551*, 204–209. https://doi.org/10.1038/nature24282.

38. Plaschka, C., Nozawa, K., and Cramer, P. (2016). Mediator Architecture and RNA Polymerase II Interaction. Journal of Molecular Biology *428*, 2569–2574. https://doi.org/10.1016/j.jmb.2016.01.028.
39. Rengachari, S., Schilbach, S., Aibara, S., Dienemann, C., and Cramer, P. (2021). Structure of the human Mediator–RNA polymerase II pre-initiation complex. Nature *594*, 129–133. https://doi.org/10.1038/s41586-021-03555-7.
40. Gorbea Colón, J.J., Palao, L., III, Chen, S.-F., Kim, H.J., Snyder, L., Chang, Y.-W., Tsai, K.-L., and Murakami, K. (2023). Structural basis of a transcription pre-initiation complex on a divergent promoter. Molecular Cell *83*, 574-588.e11. https://doi.org/10.1016/j.molcel.2023.01.011.
41. Sabari, B.R., Dall'Agnese, A., Boija, A., Klein, I.A., Coffey, E.L., Shrinivas, K., Abraham, B.J., Hannett, N.M., Zamudio, A.V., Manteiga, J.C., et al. (2018). Coactivator condensation at super-enhancers links phase separation and gene control. Science *361*, eaar3958. https://doi.org/10.1126/science.aar3958.
42. Cho, W.-K., Spille, J.-H., Hecht, M., Lee, C., Li, C., Grube, V., and Cisse, I.I. (2018). Mediator and RNA polymerase II clusters associate in transcription-dependent condensates. Science *361*, 412. https://doi.org/10.1126/science.aar4199.
43. Roeder, R.G. (2019). 50+ years of eukaryotic transcription: an expanding universe of factors and mechanisms. Nature Structural & Molecular Biology *26*, 783–791. https://doi.org/10.1038/s41594-019-0287-x.
44. Kornberg, R.D. (2005). Mediator and the mechanism of transcriptional activation. Trends in Biochemical Sciences *30*, 235–239. https://doi.org/10.1016/j.tibs.2005.03.011.
45. Harper, T.M., and Taatjes, D.J. (2018). The complex structure and function of Mediator. Journal of Biological Chemistry *293*, 13778–13785. https://doi.org/10.1074/jbc.R117.794438.
46. Friedman, L.J., Chung, J., and Gelles, J. (2006). Viewing Dynamic Assembly of Molecular Complexes by Multi-Wavelength Single-Molecule Fluorescence. Biophysical Journal *91*, 1023–1031. https://doi.org/10.1529/biophysj.106.084004.
47. Friedman, L.J., and Gelles, J. (2015). Multi-wavelength single-molecule fluorescence analysis of transcription mechanisms. Methods *86*, 27–36. https://doi.org/10.1016/j.ymeth.2015.05.026.
48. Sikorski, T.W., Joo, Y.J., Ficarro, S.B., Askenazi, M., Buratowski, S., and Marto, J.A. (2012). Proteomic Analysis Demonstrates Activator- and Chromatin-specific Recruitment to Promoters. Journal of Biological Chemistry *287*, 35397–35408. https://doi.org/10.1074/jbc.M112.391581.
49. Baek, I., Friedman, L.J., Gelles, J., and Buratowski, S. (2021). Single-molecule studies reveal branched pathways for activator-dependent assembly of RNA polymerase II pre-initiation complexes. Molecular Cell *81*, 3576-3588.e6. https://doi.org/10.1016/j.molcel.2021.07.025.
50. Rosen, G.A., Baek, I., Friedman, L.J., Joo, Y.J., Buratowski, S., and Gelles, J. (2020). Dynamics of RNA polymerase II and elongation factor Spt4/5 recruitment during activator-dependent transcription. Proceedings of the National Academy of Sciences *117*, 32348–32357. https://doi.org/10.1073/pnas.2011224117.
51. Jeon, J., Friedman, L.J., Seo, H.D., Adeleke, A., Graham, B., Patteson, E., Gelles, J., and Buratowski, S. (2023). Single-molecule analysis of transcription activation: dynamics of SAGA co-activator recruitment. bioRxiv, 2023.08.07.552353. https://doi.org/10.1101/2023.08.07.552353.
52. Sadowski, I., Ma, J., Triezenberg, S., and Ptashne, M. (1988). GAL4-VP16 is an unusually potent transcriptional activator. Nature *335*, 563.
53. Croston, G.E., Laybourn, P.J., Paranjape, S.M., and Kadonaga, J.T. (1992). Mechanism of transcriptional antirepression by GAL4-VP16. Genes & Development *6*, 2270–2281. https://doi.org/10.1101/gad.6.12a.2270.
54. Giniger, E., and Ptashne, M. (1988). Cooperative DNA binding of the yeast transcriptional activator GAL4. Proc Natl Acad Sci U S A *85*, 382–386. https://doi.org/10.1073/pnas.85.2.382.
55. Joo, Y.J., Ficarro, S.B., Chun, Y., Marto, J.A., and Buratowski, S. (2019). In vitro analysis of RNA polymerase II elongation complex dynamics. Genes Dev. *33*, 578–589. https://doi.org/10.1101/gad.324202.119.
56. Joo, Y.J., Ficarro, S.B., Soares, L.M., Chun, Y., Marto, J.A., and Buratowski, S. (2017). Downstream promoter interactions of TFIID TAFs facilitate transcription reinitiation. Genes & Development. https://doi.org/10.1101/gad.306324.117.
57. Hong, M., Fitzgerald, M.X., Harper, S., Luo, C., Speicher, D.W., and Marmorstein, R. (2008). Structural Basis for Dimerization in DNA Recognition by Gal4. Structure *16*, 1019–1026. https://doi.org/10.1016/j.str.2008.03.015.
58. Ebmeier, C.C., and Taatjes, D.J. (2010). Activator-Mediator binding regulates Mediator-cofactor interactions. Proceedings of the National Academy of Sciences *107*, 11283–11288. https://doi.org/10.1073/pnas.0914215107.
59. Jeronimo, C., and Robert, F. (2014). Kin28 regulates the transient association of Mediator with core promoters. Nature Structural & Molecular Biology *21*, 449–455. https://doi.org/10.1038/nsmb.2810.
60. Sikorski, T.W., and Buratowski, S. (2009). The basal initiation machinery: beyond the general transcription factors. Current Opinion in Cell Biology *21*, 344–351. https://doi.org/10.1016/j.ceb.2009.03.006.
61. Jean-Jacques, H., Poh, S.L., and Kuras, L. (2018). Mediator, known as a coactivator, can act in transcription initiation in an activator-independent manner in vivo. Biochimica et Biophysica Acta (BBA) - Gene Regulatory Mechanisms *1861*, 687–696. https://doi.org/10.1016/j.bbagrm.2018.07.001.
62. Bernecky, C., Grob, P., Ebmeier, C.C., Nogales, E., and Taatjes, D.J. (2011). Molecular Architecture of the Human Mediator–RNA Polymerase II–TFIIF Assembly. PLOS Biology *9*, e1000603. https://doi.org/10.1371/journal.pbio.1000603.
63. Ordabayev, Y.A., Friedman, L.J., Gelles, J., and Theobald, D.L. (2022). Bayesian machine learning analysis of single-molecule fluorescence colocalization images. eLife *11*, e73860. https://doi.org/10.7554/eLife.73860.
64. Adams, C.C., and Workman, J.L. (1995). Binding of disparate transcriptional activators to nucleosomal DNA is inherently cooperative. Mol Cell Biol *15*, 1405–1421. https://doi.org/10.1128/MCB.15.3.1405.
65. Kang, T., Martins, T., and Sadowski, I. (1993). Wild type GAL4 binds cooperatively to the GAL1-10 UASG in vitro. J Biol Chem *268*, 9629–9635.
66. Weinberg, R.L., Veprintsev, D.B., Bycroft, M., and Fersht, A.R. (2005). Comparative binding of p53 to its promoter and DNA recognition elements. J Mol Biol *348*, 589–596. https://doi.org/10.1016/j.jmb.2005.03.014.
67. Malecka, K.A., Ho, W.C., and Marmorstein, R. (2009). Crystal Structure of a p53 Core Tetramer Bound to DNA. Oncogene *28*, 325–333. https://doi.org/10.1038/onc.2008.400.
68. Soutourina, J. (2018). Transcription regulation by the Mediator complex. Nat Rev Mol Cell Biol *19*, 262–274. https://doi.org/10.1038/nrm.2017.115.
69. Tsai, K.-L., Yu, X., Gopalan, S., Chao, T.-C., Zhang, Y., Florens, L., Washburn, M.P., Murakami, K., Conaway, R.C., Conaway, J.W., et al.

(2017). Mediator structure and rearrangements required for holoenzyme formation. Nature *544*, 196–201. https://doi.org/10.1038/nature21393.

70. Plaschka, C., Hantsche, M., Dienemann, C., Burzinski, C., Plitzko, J., and Cramer, P. (2016). Transcription initiation complex structures elucidate DNA opening. Nature *533*, 353–358. https://doi.org/10.1038/nature17990.
71. Hantsche, M., and Cramer, P. (2017). Conserved RNA polymerase II initiation complex structure. Current Opinion in Structural Biology *47*, 17–22. https://doi.org/10.1016/j.sbi.2017.03.013.
72. Nozawa, K., Schneider, T.R., and Cramer, P. (2017). Core Mediator structure at 3.4 Å extends model of transcription initiation complex. Nature *545*, 248–251. https://doi.org/10.1038/nature22328.
73. Rani, P.G., Ranish, J.A., and Hahn, S. (2004). RNA polymerase II (Pol II)-TFIIF and Pol II-mediator complexes: the major stable Pol II complexes and their activity in transcription initiation and reinitiation. Mol Cell Biol *24*, 1709–1720. https://doi.org/10.1128/MCB.24.4.1709-1720.2004.
74. Kim, Y.-J., Björklund, S., Li, Y., Sayre, M.H., and Kornberg, R.D. (1994). A multiprotein mediator of transcriptional activation and its interaction with the C-terminal repeat domain of RNA polymerase II. Cell *77*, 599–608. https://doi.org/10.1016/0092-8674(94)90221-6.
75. Koleske, A.J., and Young, R.A. (1994). An RNA polymerase II holoenzyme responsive to activators. Nature *368*, 466–469. https://doi.org/10.1038/368466a0.
76. Koleske, A.J., Chao, D.M., and Young, R.A. (1996). [16] Purification of yeast RNA polymerase II holoenzymes. In Methods in Enzymology RNA Polymerase and Associated Factors Part A. (Academic Press), pp. 176–184. https://doi.org/10.1016/S0076-6879(96)73018-5.
77. Tuttle, L.M., Pacheco, D., Warfield, L., Luo, J., Ranish, J., Hahn, S., and Klevit, R.E. (2018). Gcn4-Mediator Specificity Is Mediated by a Large and Dynamic Fuzzy Protein-Protein Complex. Cell Reports *22*, 3251–3264. https://doi.org/10.1016/j.celrep.2018.02.097.
78. Zhang, F., Sumibcay, L., Hinnebusch, A.G., and Swanson, M.J. (2004). A triad of subunits from the Gal11/tail domain of Srb mediator is an in vivo target of transcriptional activator Gcn4p. Mol Cell Biol *24*, 6871–6886. https://doi.org/10.1128/MCB.24.15.6871-6886.2004.
79. Ansari, S.A., and Morse, R.H. (2012). Selective role of Mediator tail module in the transcription of highly regulated genes in yeast. Transcription *3*, 110–114. https://doi.org/10.4161/trns.19840.
80. Jeronimo, C., Langelier, M.-F., Bataille, A.R., Pascal, J.M., Pugh, B.F., and Robert, F. (2016). Tail and Kinase Modules Differently Regulate Core Mediator Recruitment and Function In Vivo. Molecular Cell *64*, 455–466. https://doi.org/10.1016/j.molcel.2016.09.002.
81. Wong, K.H., Jin, Y., and Struhl, K. (2014). TFIIH Phosphorylation of the Pol II CTD Stimulates Mediator Dissociation from the Preinitiation Complex and Promoter Escape. Molecular Cell *54*, 601–612. https://doi.org/10.1016/j.molcel.2014.03.024.
82. Ptashne, M. (2014). The Chemistry of Regulation of Genes and Other Things. J Biol Chem *289*, 5417–5435. https://doi.org/10.1074/jbc.X114.547323.
83. Sanborn, A.L., Yeh, B.T., Feigerle, J.T., Hao, C.V., Townshend, R.J., Lieberman Aiden, E., Dror, R.O., and Kornberg, R.D. (2021). Simple biochemical features underlie transcriptional activation domain diversity and dynamic, fuzzy binding to Mediator. eLife *10*, e68068. https://doi.org/10.7554/eLife.68068.
84. Hahn, S., and Young, E.T. (2011). Transcriptional regulation in Saccharomyces cerevisiae: transcription factor regulation and function, mechanisms of initiation, and roles of activators and coactivators. Genetics *189*, 705–736. https://doi.org/10.1534/genetics.111.127019.
85. Ferrie, J.J., Karr, J.P., Graham, T.G.W., Dailey, G.M., Zhang, G., Tjian, R., and Darzacq, X. (2024). p300 is an obligate integrator of combinatorial transcription factor inputs. Molecular Cell *84*, 234-243.e4. https://doi.org/10.1016/j.molcel.2023.12.004.
86. Tice-Baldwin, K., Fink, G.R., and Arndt, K.T. (1989). BAS1 Has a Myb Motif and Activates HIS4 Transcription Only in Combination with BAS2. Science *246*, 931–935. https://doi.org/10.1126/science.2683089.
87. Guarente, L., Lalonde, B., Gifford, P., and Alani, E. (1984). Distinctly regulated tandem upstream activation sites mediate catabolite repression of the CYC1 gene of S. cerevisiae. Cell *36*, 503–511. https://doi.org/10.1016/0092-8674(84)90243-5.
88. Vogel, K., Hörz, W., and Hinnen, A. (1989). The two positively acting regulatory proteins PHO2 and PHO4 physically interact with PHO5 upstream activation regions. Mol Cell Biol *9*, 2050–2057. https://doi.org/10.1128/mcb.9.5.2050-2057.1989.
89. Pomp, W., Meeussen, J.V.W., and Lenstra, T.L. (2024). Transcription factor exchange enables prolonged transcriptional bursts. Mol Cell *84*, 1036-1048.e9. https://doi.org/10.1016/j.molcel.2024.01.020.
90. Hoskins, A.A., Friedman, L.J., Gallagher, S.S., Crawford, D.J., Anderson, E.G., Wombacher, R., Ramirez, N., Cornish, V.W., Gelles, J., and Moore, M.J. (2011). Ordered and Dynamic Assembly of Single Spliceosomes. Science *331*, 1289–1295. https://doi.org/10.1126/science.1198830.
91. Agarwalla, S., Kealey, J.T., Santi, D.V., and Stroud, R.M. (2002). Characterization of the 23 S Ribosomal RNA m5U1939 Methyltransferase from Escherichia coli. Journal of Biological Chemistry *277*, 8835–8840. https://doi.org/10.1074/jbc.M111825200.
92. Johnson, A., Li, G., Sikorski, T.W., Buratowski, S., Woodcock, C.L., and Moazed, D. (2009). Reconstitution of Heterochromatin-Dependent Transcriptional Gene Silencing. Molecular Cell *35*, 769–781. https://doi.org/10.1016/j.molcel.2009.07.030.
93. Dave, R., Terry, D.S., Munro, J.B., and Blanchard, S.C. (2009). Mitigating Unwanted Photophysical Processes for Improved Single-Molecule Fluorescence Imaging. Biophysical Journal *96*, 2371–2381. https://doi.org/10.1016/j.bpj.2008.11.061.
94. Crawford, D.J., Hoskins, A.A., Friedman, L.J., Gelles, J., and Moore, M.J. (2007). Visualizing the splicing of single pre-mRNA molecules in whole cell extract. RNA *14*, 170–179. https://doi.org/10.1261/rna.794808.
95. Friedman, L.J., Mumm, J.P., and Gelles, J. (2013). RNA polymerase approaches its promoter without long-range sliding along DNA. PNAS *110*, 9740–9745. https://doi.org/10.1073/pnas.1300221110.
96. General Information — Tapqir v1.1.17+4.g318e8fc.dirty documentation https://tapqir.readthedocs.io/en/latest/info.html.
97. Wands, A.M., Wang, N., Lum, J.K., Hsieh, J., Fierke, C.A., and Mapp, A.K. (2011). Transient-state kinetic analysis of transcriptional activator·DNA complexes interacting with a key coactivator. J Biol Chem *286*, 16238–16245. https://doi.org/10.1074/jbc.M110.207589.
98. Brzovic, P.S., Heikaus, C.C., Kisselev, L., Vernon, R., Herbig, E., Pacheco, D., Warfield, L., Littlefield, P., Baker, D., Klevit, R.E., et al. (2011). The acidic transcription activator Gcn4 binds the mediator subunit Gal11/Med15 using a simple protein interface forming a fuzzy complex. Mol Cell *44*, 942–953. https://doi.org/10.1016/j.molcel.2011.11.008.